SLAC-147
UC-34
(EXP)

A SEARCH FOR UNKNOWN SOURCES OF NEUTRINO-LIKE PARTICLES*

ALLAN F. ROTHENBERG

STANFORD LINEAR ACCELERATOR CENTER
STANFORD UNIVERSITY
Stanford, California 94305

PREPARED FOR THE U.S. ATOMIC ENERGY
COMMISSION UNDER CONTRACT NO. AT(04-3)-515

May 1972

Printed in the United States of America. Available from National Technical Service, U. S. Department of Commerce, 5285 Port Royal Road, Springfield, Virginia 22151. Price: Printed Copy $3.00; Microfiche $0.95.

*Ph.D. dissertation.

ABSTRACT

A search has been made, looking for new penetrating particles that could be made by a high energy electron beam striking a target. We find no evidence for such particles. We recorded ~ 100 events induced by high energy neutrinos. These event rates are consistent with the interpretation that the neutrinos came from the decays of π and K mesons produced in the target. We set a limit on any unknown source of penetrating particles that would interact in our detector:

$$\sigma_{prod} f_{\Omega} \sigma_{int} f_{tr} < 10^{-70} \text{ cm}^4 \quad ,$$

where σ_{prod} is the photoproduction cross section on a single proton, f_{Ω} is the ratio of the production solid angle to our detector's solid angle ($\approx 3\times 10^{-3}$ sr), σ_{int} is the detectable interaction cross section per nucleon, and f_{tr} is the probability of transmission through the shield. We also set a similar limit on any unknown source of a massive penetrating particle with a finite lifetime.

$$\gamma c \tau \; e^{6.5\times 10^3 \text{ cm}/\gamma c \tau} > 2.2\times 10^{46} \text{ cm}^{-1} \sigma_{prod} f_{\Omega} f_{tr} \; .$$

ACKNOWLEDGEMENTS

I would like to express my deepest thanks to Professors Melvin Schwartz and Stanley Wojcicki, both of whom have given me some of the best experiences a graduate student could ask for. I would also like to thank Professors David Dorfan and David Hitlin for their advice and guidance.

I have had numerous helpful discussions with Dr. Y. S. Tsai and I thank him for the many calculations and programs which were used in this thesis. I would also like to thank Professor James Bjorken for the time he took to read this paper and the advice and stimulation that he gave.

I would like to thank Dr. David Fryberger, Dr. Jean-Marc Gaillard, Dr. David Kreinick, Prof. Alan Mann, and Dr. Ted Zipf who also collaborated on this experiment. Ken Johnson, Dieter Walz, and Axel Golde took a personal interest in the experiment and did the difficult job of getting the targets and the hole ready on very short notice. Dr. Arpad Barna, Dr. Dan Porat, and Roger Coombes created superscope in an incredibly short time. Don Clark, John Dickey, Evans Harrell III, Karl Hense, Dale Ouimette, Cliff Rasmussen, and E. David Uggla helped to build the superscope and set up the experiment. The operations crew under Vernon Price paid particular attention to optimizing accelerator performance during the runs.

I would like to thank my fellow graduate students Robert Piccioni and Lawrence Tankersley for their company and their help in creating this paper.

I would like to thank the people of America, who, through the N.S.F. and the A.E.C., paid for my education and living expenses and built the laboratory at which this work was done.

TABLE OF CONTENTS

LIST OF TABLES

LIST OF FIGURES

Page

I. INTRODUCTION

There are only two particles, the electron and muon neutrinos, which, although detectable, are known to pass virtually unaffected through large amounts of matter. Experiments[1] conducted at high energy proton accelerators provide the basis for our knowledge of high energy neutrinos. In these experiments neutrinos are produced by the decay of pions and kaons which were created by the strong interaction between hadrons. The experimental search described in this paper was done to answer two questions. 1) Are there any other particles, besides the neutrinos, which can be produced at a high energy electron accelerator, penetrate large amounts of matter, and be detected? 2) Since electromagnetic processes play a more important role at an electron accelerator, are there any other sources of neutrinos of sufficient magnitude to change the number or appearance of neutrino interactions at such a machine, as compared to a proton accelerator?

We can consider the basic experimental approach as a combination of three parts; the production of particles by the electron beam striking a target, the passage of these particles or their decay products through a massive shield, and the detection of particles on the far side of the shield.

When a high energy electron passes through a target it loses energy by the emission of high energy photons (bremsstrahlung). These photons can then produce electron-positron pairs in the Coulomb field of the target nuclei. These two processes are responsible for the electron-photon cascade that develops in such a situation. Although most of the original electron's energy remains in this part of the shower, other high energy particles can be produced, by either the electrons or the photons. Direct photoproduction was more important than electroproduction in our experiment because we used thick, many radiation length targets and an electron can only contribute to electromagnetic production of secondary particles by the emission of a virtual photon. The spectrum of virtual photons from an electron is equivalent to the real bremsstrahlung spectrum which would be produced by that electron in a 0.02 radiation length target.[2] This argument only applies to electromagnetic processes. There remains the possibility that electrons might interact in some new way to produce a secondary particle.

The high energy photons in a shower are known to produce secondary particles by a number of mechanisms. Any particle that has an electromagnetic form factor can be photoproduced by pair production (Fig. 1). This process is responsible for the electron-positron pairs mentioned above and is also the mechanism for the direct production of muons. Strongly interacting particles can be produced in other ways. Mesons and baryons can be produced by the exchange of one or more such particles with the target nucleus (Fig. 2). In any of these processes the fragmentation of the excited target can produce additional secondary particles. Production of mesons with the same quantum numbers as a photon, the ρ, ω, and ϕ, is particularly large. π and K mesons come from the decays of these mesons and from direct production. In all of these cases, the secondary particles come out in a narrow cone along the direction of the photon's momentum.

To increase the sensitivity of our experiment, we wanted to enhance the production of secondary particles. A high energy electron makes more energetic and more numerous photons than a less energetic electron. Also, a high energy photon can more readily produce a massive particle than can a low energy photon. Therefore, we used as high an incident electron energy and as much current as possible. We made the target sufficiently thick (> 2 r.l.) so that most of the high energy photons in the shower could contribute to the secondary particle production. Production could also be enhanced by an appropriate choice of target material. We used several different targets to vary the amount of photoproduction and the degree to which mesons would be absorbed before they decayed.

As is the case at the proton accelerators, the decays of pions and kaons are a source of high energy muon neutrinos. Since similar numbers of positive and negative mesons were produced, we had approximately equal numbers of neutrinos and antineutrinos. The decay probability of a high energy meson within a thick target of several interaction lengths is small. For aluminum, the interaction length for a meson is ~ 0.40 m, while the decay length for a 4 GeV π is 220 m and for a 4 GeV K is 30 m. The neutrino flux could be enhanced by increasing the mean free path of the mesons. This was done during part of the experiment by using a small target upstream of the main target and shield, allowing the mesons to decay in the intervening air space. This mode of running allowed us to calibrate the sensitivity of the apparatus since neutrino production in such a configuration was already understood. It also served as a comparison point for anomalous neutrino production.

The shield had to be sufficiently thick to stop all of the known particles, except for neutrinos. The high energy muons produced in the target had the greatest penetrating power. Since they only interacted electromagnetically, they slowly lost their energy by scattering and eventually decayed or were captured. There were some inelastic collisions and the muons could knock out neutrons from the nuclei they struck. The shield had to stop all of these particles too. Thus, it was made somewhat thicker than the range of the highest energy muons. We did not want to make it much thicker than this since that would have reduced the solid angle of our detector and also possibly increased the amount of absorption of any unknown penetrating particle.

Particles passing through the shield were detected by their interactions in a detector on the far side of the shield. The detector was centered on the same line as the original electron beam to take advantage of the collimation inherent in the production process. Since we were interested in seeing events induced by particles with very small interaction cross sections ($\approx 10^{-38}$ cm^2 for a neutrino on a proton), we wanted a very massive detector. Even with a multiton detector one could only expect a few events each day. Therefore, we used optical spark chambers with scintillation counters to provide the event trigger. The chambers were pulsed and pictures were taken when the counters indicated the passage of a charged particle which might have come from an interesting event.

II. THEORY AND SPECULATION

Electromagnetic Production of Massive Particles

Any particle that has an electromagnetic form factor can be produced in pairs by a photon in the electromagnetic field of a nucleus. The diagrams for this process are shown in Fig. 1. We used an improved Weizsacker Williams method,[3] due to Kim and Tsai, to calculate the differential pair production cross section. This method properly handled the atomic and nuclear form factors. When the minimum momentum transfer was greater than or comparable to the internucleon distance in a target nucleus, these form factors caused a large decrease in the cross section. The Weizsacker Williams method was an approximation scheme in which the matrix elements were calculated assuming that both photons were real. When compared to the exact calculation using the Born approximation, agreement was found to a few percent. These differential cross sections were integrated to give the total cross section.

For the energy angle distribution we used,

$$\frac{d\sigma}{d\Omega\, dp} = \frac{\alpha^3}{\pi k}\left(\frac{E^2}{m^4}\right) \quad \frac{x(1-x)}{(1+\ell)^2}\left(L^{\mu\nu} g_{\mu\nu}\right)_{\theta_+=0} X$$

$$\alpha = \frac{1}{137}$$

k = photon energy

E = particle energy

m = particle mass

$$x = \frac{E}{k}$$

$$\gamma = \frac{E}{m}$$

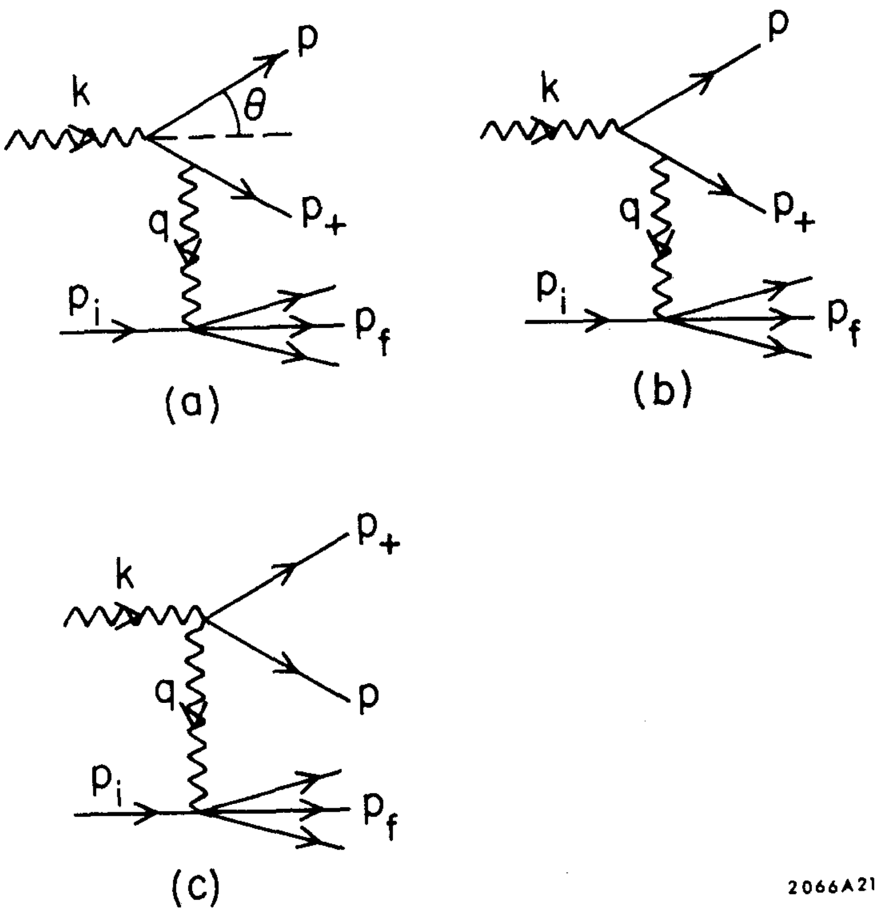

FIG. 1--Pair production. Diagram c does not contribute for spin 1/2 particles.

$$\ell = \gamma^2 \theta^2$$

$\left(L^{\mu\nu} g_{\mu\nu}\right)_{\theta_+ = 0}$ = the matrix element squared

X = the integral over the form factors .

The form of the factor $\left(L^{\mu\nu} g_{\mu\nu}\right)_{\theta_+ = 0}$ depends on the type of particle being produced:

$$\left(L^{\mu\nu} g_{\mu\nu}\right)_{\theta_+ = 0} = \frac{2}{x(1-x)} \left(1 - 2x + 2x^2 + \frac{4x(1-x)\ell}{(1+\ell)^2}\right)$$

for spin 1/2 charged particles

$$= 2 \frac{(1+\ell^2)}{(1+\ell)^2} \quad \text{for spin 0 charged particles}$$

$$= \kappa \frac{(1+\ell)^2}{4x(1-x)} \quad \text{for spin 1/2 neutral particle}$$

with anomalous moment $\kappa \frac{e}{2m}$

In all of these cases we can see that the typical angle for production is given by ℓ=1 which implies that $\theta \approx m/E$. The characteristic size of the cross section is $\alpha^3/m^2 \approx 10^{-34}/m^2\ cm^2 - GeV^2$.

The expression for X was

$$X = \frac{1}{2M_i} \int_{t_{min}}^{m^2(1+\ell)^2} \frac{dt}{t^2} \int_{M_i^2}^{(u-m)^2} dM_f^2 (t - t_{min})\, W_2(t, M_f^2)$$

M_i = mass of target

M_f = mass of final state

$t = -q^2$

$$t_{min} \simeq \frac{(k \cdot p)^2}{(k-E)^2} + \frac{(k \cdot p)\left(M_f^2 - M_i^2\right)}{M_i(k-E)}$$

$$u = \left[(k+p_i-p)^2\right]^{1/2} = \left[M_i^2 + m^2 + 2(k-E)\, M_i - 2\, k \cdot p\right]^{1/2}$$

$W_2(t, M_f^2)$ = one of the two electron scattering form factors[4]

The form used for W_2 depended on the value of t_{min} for the process (Table I). For pair production of very light particles, such as electrons, we used the form factor for the screened nucleus and that for the scattering of atomic electrons screened by the nuclear charge. For higher values of t_{min}, such as for muon pairs, the atomic electrons were ignored and an elastic nuclear form factor was used for coherent (Z^2) production. When $t_{min}^{1/2}$ was larger than or comparable to the internucleon distance, incoherent (Z, A) production was also included. A Pauli suppression factor was included in the quasi-elastic form factor. The inelastic contribution to the incoherent production was negligible. When the incoherent production dominated the coherent production, targets with small Z yielded more particles than large Z targets of the same radiation length.

Production of Mesons

We examined two of the many possible ways in which π's could be produced by photons. One of these was by the Drell process[5] (Fig. 2a), a single pion exchange diagram. The production cross section was found to be large for an almost real exchanged pion, where the denominator of the propagator for the intermediate pion vanishes. In that situation, the contribution of the pion nucleon vertex was expressed in terms of the total

TABLE 1

Electromagnetic Form Factor for Nuclear Targets

$(t_{min})^{1/2} \approx 10^{-3}$ GeV

$$W_2 = 2M_i\,\delta(M_f^2 - M_i^2)\,Z^2 \frac{a^4 t^2}{(1+a^2 t)^2} + 2\,M_i'\,\delta(M_f^2 - M_i'^2)\,Z \frac{a'^4 t^2}{(1+a'^2 t)^2}$$

$$M_i = A\,M_p \qquad a = 111/(m_e\,Z^{1/3})$$

$$M_i' = m_e \qquad a' = 1440/(2.718)^{1/2}/(m_e\,Z^{2/3})$$

$(t_{min})^{1/2} \approx 10^{-1}$ GeV

$$W_2 = 2M_i\,\delta(M_f^2 - M_i^2)\,Z^2/(1 + \frac{t}{d})^2$$

$$M_i = A\,M_p \qquad d = 0.164A^{-2/3}\,\mathrm{GeV}^2$$

$(t_{min})^{1/2} \gtrsim 10^{-1}$ GeV

$$W_2 = \frac{2M_p\,\delta(M_f^2 - M_i^2)}{(1+t/.71)^4}\,C(t)\left[Z\left(\frac{1+2.79^2\,\frac{t}{4M_p^2}}{1+t/4M_p^2}\right) + (A-Z)\left(\frac{1.41^2\,\frac{t}{4M_p^2}}{1+t/4M_p^2}\right)\right]$$

$$M_i = M_p$$

$$C(t) = 1 \qquad \text{if } Q = \left(\frac{t^2}{4M_p^2} + t\right)^{1/2} > 2p_F = 0.50\ \mathrm{GeV}$$

$$C(t) = \frac{3}{4}\,\frac{Q}{p_F}\left(1 - \frac{1}{12}\left(\frac{Q}{p_F}\right)^2\right)$$

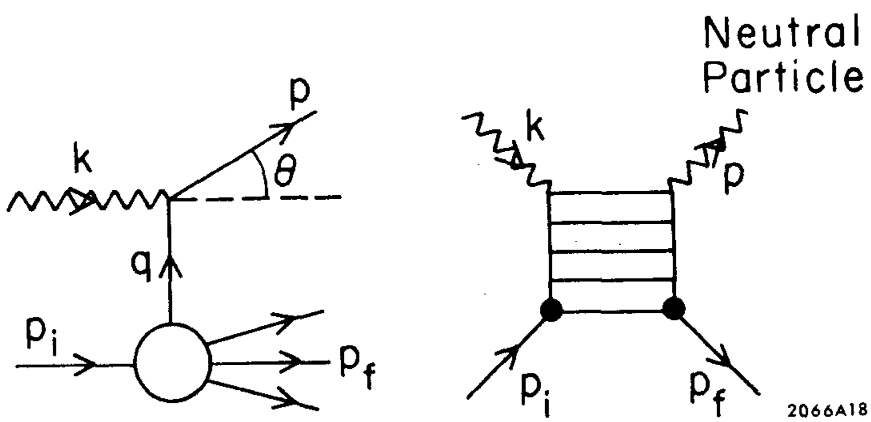

FIG. 2--Some diagrams for the production of strongly interacting particles.
(a) Single particle exchange, (b) diffraction production.

π-nucleon cross section:

$$\frac{d^2\sigma_{\pi^\pm}}{dE d\Omega} = \frac{\alpha}{8\pi^2} \frac{E(k-E)}{k^3} \frac{\sin^2\theta}{(1-\beta\cos\theta)^2} \sigma_{\pi^\mp+A,\,\text{total}} (k-E)$$

$$\beta = \frac{p}{E}$$

$$\sigma_{\pi^\mp+A,\,\text{total}} = A^{2/3}\, 45 \times 10^{-27}\ \text{cm}^2$$

As before, the characteristic production angle was $\theta \approx m/E$, but the cross section is $\approx 10^{-31}\ \text{cm}^2$.

We considered π's produced by the decay of the ρ.[6] For the ρ production we used.

$$\left.\frac{d\sigma}{d\Omega}\right)_{c.m.} = C\, p^2_{\rho\, c.m.}\ A^{1.63}\, e^{BA^{2/3}t}$$

$$C = 3.0 \times 10^{-29}\ \text{cm}^2\ \text{GeV}^{-2}\ \text{sr}^{-1}$$

$$B = -10\ \text{GeV}^{-2}$$

The ρ does not decay isotropicly in its rest frame. We assumed a $\sin^2\beta$ angular distribution, where β is the angle between the π in the ρ rest frame and the direction of the ρ in the center-of-mass system.

In our calculations these two processes did not give very satisfactory results when compared to the experimental data. They completely neglected the meson yield from the excited nucleon final state. Also, there were many other processes which contributed to the total yield. Therefore, we used a phenomenological model to get the pion yields. The same thing was true for the production of K's. The production of ϕ's, which decay into K's, was similar to ρ production. The Drell model was not very believable for the large mass of the K, since the denominator of the propagator is $\approx m_K^2$ and not 0.

Neutrinos and Their Interactions

Our understanding of weak interactions is based on a phenomenological theory. All of the interactions directly observed up to now can be described by the complete effective Lagrangian.

$$\mathscr{L}_{eff} = \frac{G}{\sqrt{2}} J_\lambda^+ J^\lambda + \begin{matrix}\text{hermitian} \\ \text{conjugate}\end{matrix} \qquad J_\lambda = J_\lambda^{(h)} + J_\lambda^{(u)} + J_\lambda^{(e)}$$

where $G = 10^{-5}/M_p^2$. This also allows diagonal interactions which have not been observed yet. The muon and electron currents are given by,

$$J_\lambda^{(u),(e)} = \bar{\psi}_{\mu, e}(x)\, \gamma_\lambda (1-\gamma_5)\, \psi_{\nu_\mu, \nu_e}(x)$$

$J_\lambda^{(h)}$ is a current constructed from hadron fields. This theory yields excellent results for calculations in which only the lowest order diagrams are included. The effective Lagrangian is often considered as the low energy limit of an interaction mediated by an intermediate vector boson. In that case,

$$\mathscr{L}_{IVB} = g_W J_\lambda W^\lambda + \begin{matrix}\text{hermitian} \\ \text{conjugate}\end{matrix}$$

where $g_W^2/M_W^2 = G/\sqrt{2}$. For high energy neutrino interactions, such as

$$\nu_\mu + n \rightarrow p + \mu^-$$

the characteristic cross section is $G^2 M_p^2 \approx 10^{-38}$ cm^2. This is not the only process that can occur and as the neutrino energy rises more channels open up, increasing the total cross section.

The forms of the Lagrangian used above predict an electromagnetic form factor for the neutrino (Fig. 3). The cross section for neutrino pair production in a Coulomb field,[7] using $\mathscr{L}_{\mathrm{eff}}$, is

$$\sigma = Z^2 \alpha^3 \left(\frac{k}{m_\ell}\right)^6 \cdot 1.25\times 10^{-49}\ \mathrm{cm}^2$$

where m_ℓ is the mass of the lepton in the intermediate state. This result is a considerable overestimate for high energy photons because of the form factor used. However, it gives cross sections of $\approx 10^{-43}\ \mathrm{cm}^2$ for 10 GeV photons to make muon neutrinos from a proton. This is much too small for us to detect in this type of experiment.

We can abandon our effective Lagrangian and ask what the experimental limits are on neutrino form factors. These results are summarized in Table II.[8] Some of these limits are set on the basis of neutrino experiments that have considerably more data than our experiment. The only way we could hope to improve on these limits is by being sensitive to the form factor in the production of neutrinos. Unfortunately, this is a hopeless task for us. It will be shown later that our sensitivity was $\sigma_{\mathrm{prod}}\sigma_{\mathrm{int}} \approx 10^{-70}\ \mathrm{cm}^4$. Thus, the lowest neutrino production cross section we could detect would be $\sigma_{\mathrm{prod}} \approx 10^{-32}\ \mathrm{cm}^2$. This is much more than the $10^{-38}\ \mathrm{cm}^2$ cross sections that detection experiments are sensitive to. If we had a pair production cross section of this magnitude there would also be a bremsstrahlung cross section of approximately the same size and this would have already been observed.

Heavy Leptons

There has been considerable speculation as to the possible existence of leptons other than the eight already known. In particular, we would like to

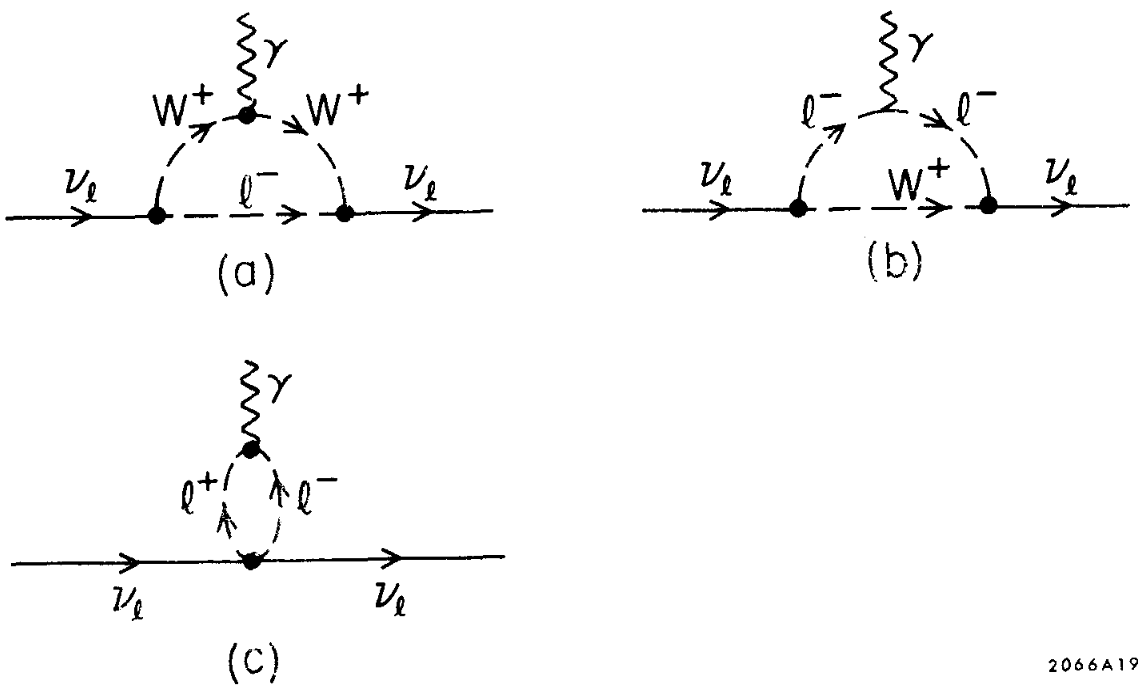

FIG. 3--Diagrams for the electromagnetic form factors of the neutrino. (a, b) IVB theory, (c) effective theory.

TABLE II

Summary of the Known Limits for the Electromagnetic Interactions of Neutrinos

Property	ν_e	ν_μ
Charge	$<4\times 10^{-17}$e from charge conservation	$<10^{-13}$e from astrophysics, if $m_\nu < 1$ keV
	$<10^{-13}$e from astrophysics	$<3\times 10^{-5}$e from charge conservation
	$<3\times 10^{-10}$e from electron-neutrino scattering	$<3\times 10^{-5}$e from pion production by neutrinos
Magnetic moment (in Bohr magnetons)	$<10^{-10}$ from astrophysics	$<10^{-10}$ from astrophysics, if $m_{\nu_\mu} < 1$ keV
	$<1.4\times 10^{-9}$ from neutrino-electron scattering	$<10^{-8}$ from pion production by neutrinos
Charge radius (in cm)	$<4\times 10^{-15}$ from electron-neutrino scattering	$<10^{-15}$ from pion production by neutrinos
	$<4\times 10^{-14}$ from astrophysics	$<4\times 10^{-14}$ from astrophysics, if $m_{\nu_\mu} < 1$ keV

consider the case of a lepton with $m_H > m_\mu$, having its own neutrino, ν_H, and their two antiparticles.[9] It could be included in our effective Lagrangian by simply adding the following additional piece to the current.

$$J_\lambda^{(H)} = \bar{\psi}_H(x)\, \gamma_\lambda\, (1-\gamma_5)\, \psi_{\nu_H}(x)$$

The principal restriction on the existence of this heavy lepton is $m_H > m_K$ since the K is not observed to decay into such a particle. Experiments[10] have been done to look for heavy leptons, but none of them would have seen this particular type.

Our experiment was originally proposed to look for such a particle.[11] The heavy lepton could be pair produced by the electron beam in our target. This can be calculated by the method outlined previously. It would decay almost immediately, $\approx 10^{-10}$ sec, and the ν_H would penetrate the shield and interact in our detector. The event signature would be distinctive since there would be only a small probability, $\sim 20\%$, of having a muon in the final state. The lifetime and branching ratios of these particles have been calculated by Tsai[12] and are given in Table III.

New Types of Long Range Interactions

There is another highly speculative kind of penetrating particle that can be considered.[13] We can ask if there is a long range interaction that couples to strange particles, similar to the electromagnetic interaction between charged particles. Such an interaction would result in a force between two strange particles. It would be mediated by a "photon", a zero mass field similar to ordinary light, that would couple to two strange particles. Our experiment could conceivably detect a "photon" which was produced in the beam dump, penetrated the shield, and interacted in the detector producing a strange particle.

TABLE III

Lifetimes and Branching Ratios of Heavy Leptons

m (GeV)	.3	.4	.5	.6	.7	.8	.9	1.0
Lifetime (sec)	1.0×10^{-9}	3.1×10^{-10}	1.3×10^{-10}	6.6×10^{-11}	3.6×10^{-11}	2.1×10^{-11}	1.0×10^{-11}	5.4×10^{-12}
$\frac{\Gamma \rightarrow (\ell \rightarrow \nu\nu e)}{\Gamma\ (\text{total})}$	8%	11%	14%	18%	21%	23%	20%	19%
$\frac{\Gamma(\ell \rightarrow \nu\nu\mu)}{\Gamma\ (\text{total})}$	4%	7%	11%	12%	18%	20%	18%	17%
$\frac{\Gamma(\ell \rightarrow \pi\nu)}{\Gamma\ (\text{total})}$	88%	82%	75%	68%	61%	52%	37%	28%
$\frac{\Gamma(\ell \rightarrow \rho\nu)}{\Gamma\ (\text{total})}$	0	0	0	0	0	4%	25%	36%

We will assume a generalized model of such a long range interaction. Our "light" will interact with a massive charged particle, the A, with a coupling constant α'. We assume that it does not interact with any other particles. We get this result if we assume that the A also has a "charge" while the "charge" of all other particles is 0. The form of the interaction will otherwise be exactly the same as that in quantum electrodynamics. For the case of strangeness the A might be the K meson, the least massive of the strange particles.

Depending on the other interactions of the A, there are several ways in which a photon could produce a "photon" in the field of a nucleus. As a first attempt, we will assume that the A does not interact strongly. The appropriate diagram (Fig. 4a) is that for Delbrück scattering.[14] We can get a very good estimate for the forward differential cross section in terms of the total pair production cross section for A pairs. We use the optical theorem, assuming the real part of the amplitude to be small compared to the imaginary part, to write,

$$\frac{d\sigma_{\gamma \to \gamma'}(\theta=0)}{d\Omega} = \frac{\alpha'}{\alpha} \frac{k^2}{(4\pi)^2} \sigma_{\text{pair}}^2 \approx \frac{\alpha'}{\alpha} \cdot 7\times 10^{-37}\,\text{cm}^2$$

.5/10 = .05

$$\begin{pmatrix} k=10, \quad m_A=0.5, \quad Z=13 \\ \sigma_{\text{pair}} = 1.6\times 10^{-33}\,\text{cm}^2 \end{pmatrix}$$

for the cross section per nucleon. The characteristic production angle for the process is $\theta \approx m_A/k$. The contribution of the diagram shown in Fig. 4b vanishes by Furry's theorem if the "photon" is odd under charge conjugation. If we relax this assumption we would expect the cross section to rise by a factor of $(\alpha Z)^{-2}$. We can also produce the γ', in either case, by pair

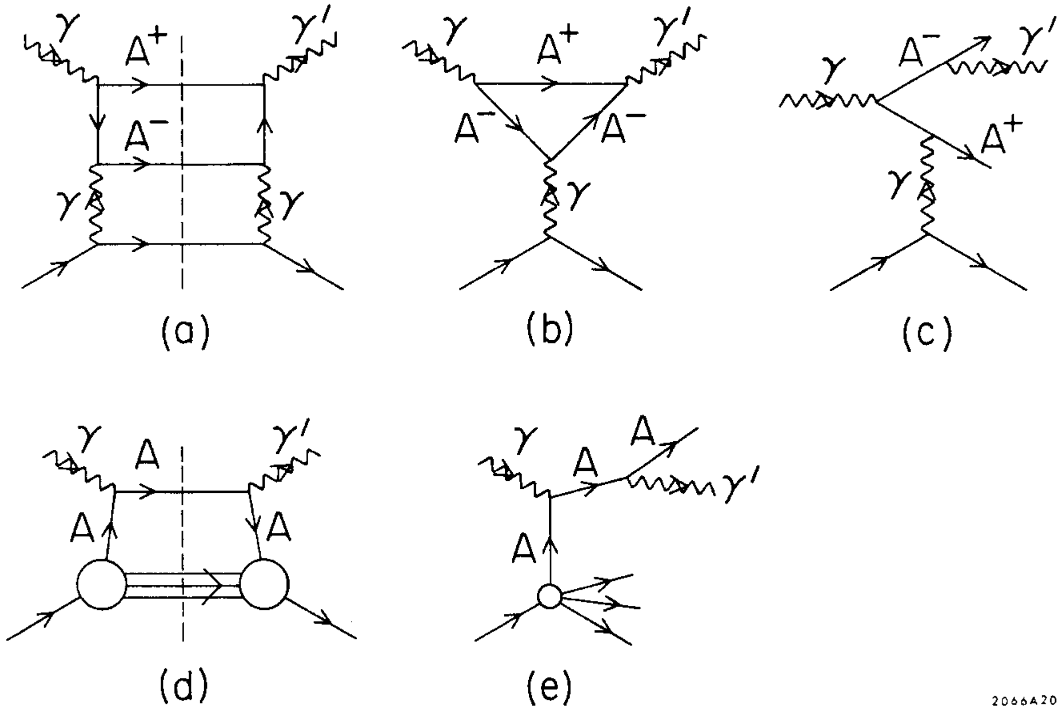

FIG. 4--Diagrams for the production of "light" by light.

production with bremsstrahlung (Fig. 4c). This will have the same cross section as the diagram just calculated.

If we allow the A to be strongly interacting as in the strangeness case, there are many diagrams, including Figs. 4d and 4e, which become important. A simple coupling constant argument suggests that these cross sections would be greater than the Delbrück case by a factor $f^2/(\alpha Z)^4$, with $f \approx 15$. We can also estimate diagram d using the optical theorem,

$$\frac{d\sigma_{\gamma \to \gamma'}(\theta=0)}{d\Omega} = \frac{\alpha'}{\alpha} \frac{k^2}{(4\pi)^2} \sigma^2_{\gamma p \to A + \text{anything}} \approx \frac{\alpha'}{\alpha} 3 \times 10^{-31} \text{cm}^2$$

$$(k=10,\ A \approx K^+,\ \sigma_{\gamma p \to K^+} = 12\ \mu b)$$

Except for the case of strangeness, the choice of which particle the A is, cannot be made. However, we can evaluate the cross section using the experimentally measured values for K and A2 mesons. We probably should not use the result for ρ's since they are known to have the same quantum numbers as the photon. We can calculate diagram e by using the same approximation as for the Drell process. We get,

$$\frac{d\sigma_{\gamma \to \gamma'}(\theta'=0)}{dk' d\Omega'} = \frac{\alpha'}{\alpha} \frac{\alpha^2}{320\pi^3} \frac{(k-k')^3}{k' k\, m_A^2} \sigma_{A+p,\text{total}}$$

$$\frac{d\sigma_{\gamma \to \gamma'}(\theta'=0)}{d\Omega'} \approx \frac{\alpha'}{\alpha} \frac{\alpha^2}{320\pi^3} \frac{k^2}{m_A^2} \sigma_{A+p,\text{total}} \approx \frac{\alpha'}{\alpha} 4 \times 10^{-32} \text{cm}^2$$

$$(k=10,\ m_A = 0.5,\ \sigma_{A+p} = 25\ \text{mb})$$

As before the characteristic production angle will be $\theta \approx m_A/k$.

Detection of such particles also depends on the interactions of the A. If the A does not interact strongly, the signature will be an $A^+ - A^-$ pair produced in the field of a nucleus. If it does interact strongly we can have single A production with a cross section $(\alpha'/\alpha)\ \sigma_{\gamma p \rightarrow A + \text{anything}}$. Both of these processes have signatures which cannot be confused with the muon signature in ordinary neutrino events.

III. APPARATUS

The experimental program outlined in the previous sections is obviously speculative with a reasonable chance of yielding no positive results. This fact combined with the costs of implementing a high energy physics experiment led to many compromises in design and operation. Many changes and additions were made to the apparatus during the three running periods, dictated in large part by the excitement generated by some of the preliminary results.

The experiment was done at the Stanford Linear Accelerator Center. It was located in the main electron beam line in the area behind End Station A (Fig. 5). The full electron beam was directed onto targets or the beam dump under the hill. The bulk of the hill served as the shield. Our detection apparatus was located in a hole behind the hill, in line with the electron beam.

Primary Beam

The electron beam was used at maximum energy and intensity. Typical beam parameters were 19 GeV electron energy, 50 - 60 mA current for 1.5 microseconds, and a repetition rate of 330 pulses per second. This meant $\sim 1.8\times10^{14}$ electrons/sec or 2.5 coulombs/(very good) day. During most of the first running period, there was an experiment in End Station A and we operated in a parasitic mode, in which we had a lower repetition rate, energies between 12 and 20 GeV, and currents of 30 - 60 mA.

The beam current was monitored by toroids just in front of the dump, at the upstream end of End Station A, and at other upstream points. The steering of the beam was checked visually with a television picture of the

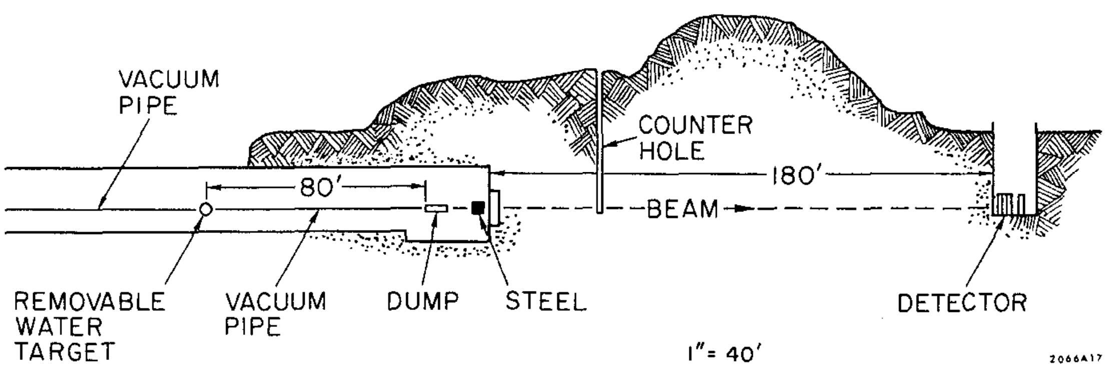

FIG. 5--Overall view of experiment.

beam hitting a screen directly in front of the target position. The position of the beam at the dump could be checked with a secondary emission monitor. There were also many safety devices that automatically shut down the machine if this high energy beam, or any significant fraction of it, was incorrectly steered. Thus, the beam did not deviate from the theoretical line by more than one milliradian.

For part of the experiment, the time at which the beam hit the dump could be measured to several nanoseconds. This was done by placing a small scintillation counter in a beam level hole approximately 40 feet in back of the dump.

Production Configurations

Several different production configurations were used during the course of the experiment. One design objective was to be sensitive to unknown particles while restricting the known flux of neutrinos. This was done by absorbing the π's and K's that decay into neutrinos. A low Z and A material is best suited for photoproduction and a high density will increase the absorption at a given A. We used the beam dump, a large tank of water, as the target for the first two runs. At one point in the second run we put a three radiation length block of tantalum directly in front of the dump, in order to decrease the amount of photoproduction and shorten the interaction length. This drastically cut the ordinary neutrino flux. Unfortunately, any other coherent photoproduction process should also have been suppressed. During the third run, the water dump was replaced with an aluminum sphere dump. This was a collection of closely packed spheres cooled by circulating water. It was 75% aluminum and 25% water by volume. The neutrino flux from this dump was also expected to be lower than that from the water dump. Both of these dumps were large enough to completely contain the beam shower. The smaller aluminum dump was 10 inches in diameter and 7 feet long. This was over 24 radiation lengths or 7 interaction lengths.

The neutrino calibration was done with a 30 inch, 2 radiation length water target located 80 feet upstream of the dump. Thus a high energy pion or kaon produced in the target was approximately 80 times more likely to decay in this configuration than if it were in the aluminum dump. There was a two-foot-diameter iron vacuum pipe with a 1/4-inch-thick wall extending from the target to the dump.

Shielding

Most of the shielding was provided by the 180 feet of rock in the hill. It is a miocene sandstone with density 2.0 gm/cm^3. Its composition is roughly 70% quartz and 30% feldspar.[15] If we assume it is simply SiO_2 and use a strong interaction cross section of 45.3 $A^{2/3}$ mb,[16] we get a collision length of 100 gm/cm^2. Thus, the rock represented 11,000 gm/cm^2 of SiO_2 or 110 interaction lengths. Depending on the time of year, there can be an additional 15% of water which means 820 gm/cm^2 or another ten interaction lengths. For the third running period there were 5.75 feet of steel immediately after the dump. This was another 1400 gm/cm^2 or 10 interaction lengths. The amount of rock alone was sufficient to stop muons with energies below 22 GeV.[17] The effect of the iron was an additional 2.3 GeV stopping power. In this configuration a 19.5 GeV muon would stop at least 42 feet from the back of the shield. This means that even neutrons that were made by muons at the very end of their range would be attenuated, by a factor of $e^{-25} \approx 10^{-11}$, by the time they reached the detector.

Detection Apparatus

The detector consisted of four spark chambers, each weighing five tons, and up to three scintillation counter banks (Fig. 6). They occupied the bottom of a 37 foot deep, 16 foot diameter hole that was dug behind the hill. Three of the chambers were kept together and composed the interaction region. The fourth one was located 16 inches further downstream for the first two running periods and 34 inches further down for the final running period. This change was done to make time-of-flight measurements easier for the first two counter banks. The counter banks were as follows: the A bank immediately downstream of the three chambers, the B bank just before the fourth chamber, and the C bank just after the fourth chamber.

The chambers were the ones used in the second Brookhaven neutrino experiment[18] and a K_L^o charge asymmetry experiment at SLAC.[19] Each module was 8×8 feet in cross section and had 11 one-inch aluminum plates. A minimum ionizing particle would lose 14 MeV in each plate. The total thickness of the four modules was 2.7 interaction lengths. The plates were separated by 3/8-inch lucite frames with the one optically polished surface on top. Typically, a 90 - 10% mixture of neon-helium was used in the chambers. This was purified by being recirculated through a liquid nitrogen cold trap and a molecular sieve. Unfortunately, during the first two runs, the first chamber leaked so severely that it had to be placed on a non-recirculating helium supply. This made its track quality and multitrack efficiency somewhat worse and its memory time longer, compared to the other chambers. The chambers were powered by a capacitor spark gap system. During the final running period, a 50-volt dc clearing field was applied to the chambers to reduce the memory time.

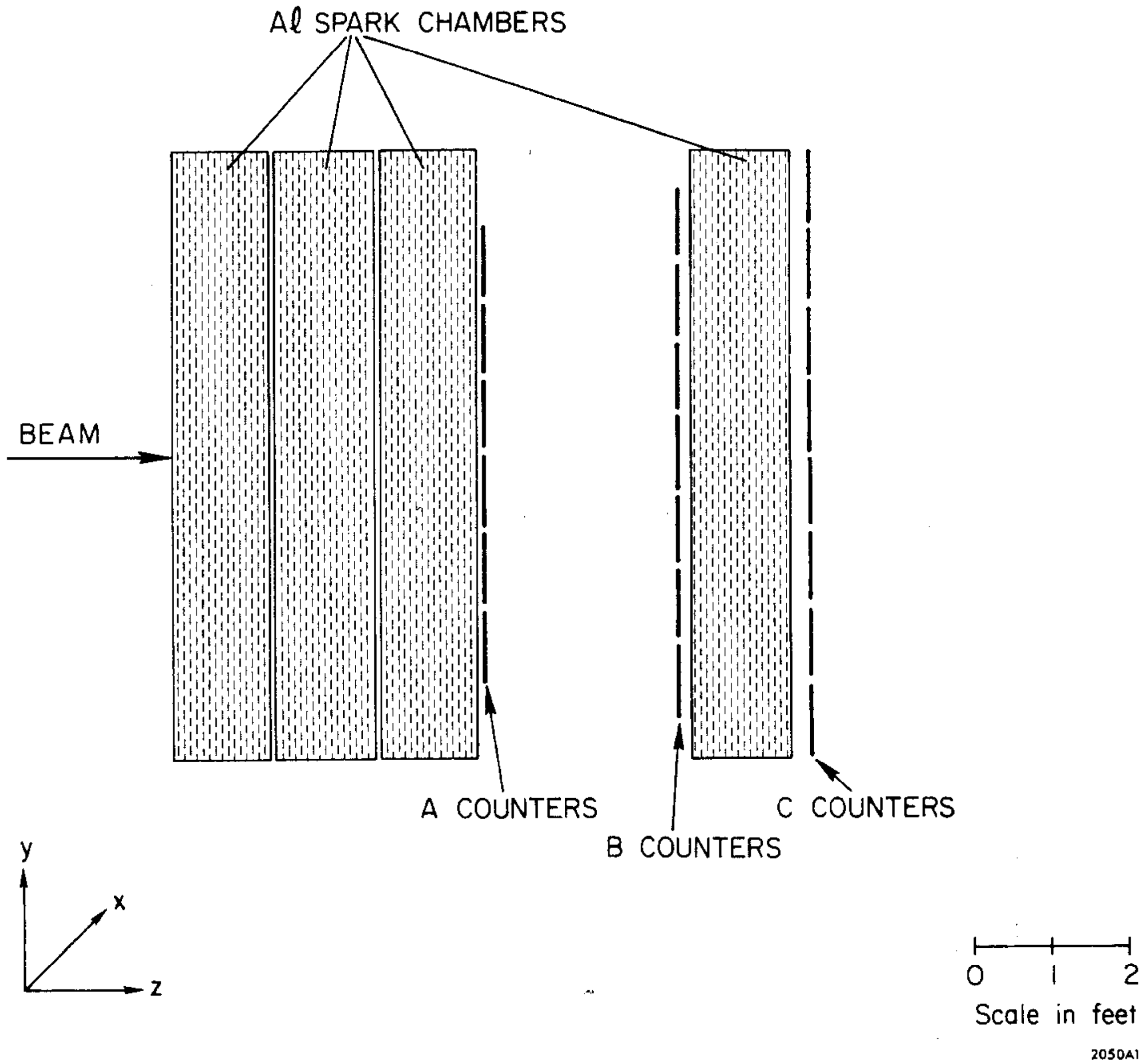

FIG. 6--Detection apparatus.

The chambers were viewed in stereo with a 15° angle between the two lines of sight. A set of optical prisms at the top of each module allowed us to see through each of the four modules from a single point. A prism and mirror system allowed us to place both views onto a single 70 mm film frame. The camera and mirror system were located on the mezzanine, 20 feet above the bottom of the hole. The camera used 400-foot rolls of Plus-X film. A six-digit frame number and the time of day were present on each picture. Three flash tube fiducial lights were located at the lens plane during the final run.

The counters used were also relics of previous experiments. They were 11 inches wide, 1/2-inch thick, and 8 or 9 (one was 10) feet long, and were viewed by 56AVP phototubes at each end. During the final running period, they all had Monsanto MV10 light emitting diodes mounted in their centers. The configuration of the counter banks varied among the running periods. During the first, there were 6 A counters and 7 C counters. The second period had 6 A counters, 7 B counters, and 2 C counters. The final configuration was 6 A counters, 7 B counters, and 8 C counters. The counters were installed horizontally. In all cases the counter banks were staggered in the vertical dimension so that the center of one counter was at the same height as the edges of the one or two counters in the adjacent banks. During the third running period, a 3/4-inch wooden wall was placed just upstream of the B bank in order to reduce the A-B accidental trigger rate.

Logic

The counter trigger requirement was two counters, one from each of two adjacent banks, consistent with a particle passing horizontally through the detector. A counter was said to have fired if the phototubes on each end had signals above threshold no more than 12 nsec apart. Threshold was set well below the minimum ionizing level. This trigger was sensitive to horizontal tracks and rejected some of the tracks associated with cosmic rays. The trigger was sensitive to tracks emerging from the group of three chambers and also to the possible decay of a neutral particle in the gap between the chambers. To cut down on the number of cosmic ray triggers we demanded that the trigger occur during the 1.5 microsecond machine pulse. There was also a deadtime requirement so that the chamber capacitor banks could recharge and for the camera film advance.

A logic diagram is given in Fig. 7. The total number of pulses, the number of gated pulses, the total number of triggers, and the number of each type of trigger was displayed on scalers and allowed us to monitor the counters and logic. During the final run, the superscope, its calibration system, and the light emitting diodes made the calibration and testing of the counters and logic a very simple procedure.

Superscope

After the first two running periods it was decided that we needed a good way to determine the number of single-prong neutrino events occurring in the first three modules. This signal was contaminated by the tracks of cosmic ray muons that entered from the downstream side, triggered the system, and came to a stop within the first three chambers. Analysis of the vertical angle distribution did not seem to be an effective way to separate these contributions. However, if we knew the direction of travel of these particles, as determined by time-of-flight, the separation would be easy.

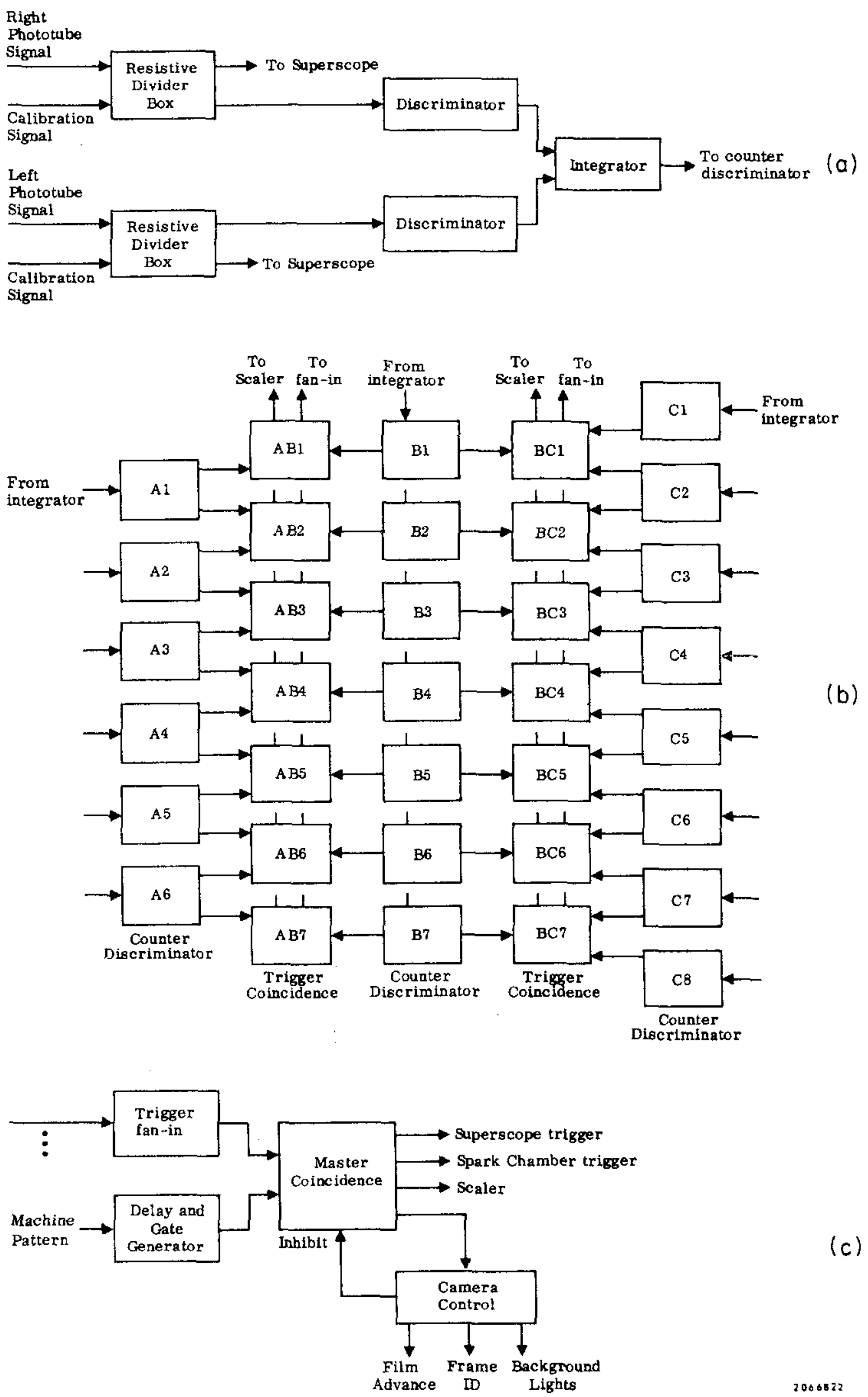

FIG. 7--Logic diagram. (a) Counter logic, (b) trigger logic, (c) master coincidence.

It was also hoped that detailed knowledge of the timing and pulse shape of the counter signals in unusual events would be helpful. For these reasons we decided to display every phototube signal on a high speed oscilloscope and record the traces on film after each trigger. The product of these desires was "superscope", a 48-channel nanosecond oscilloscope system.*

*For a description of "superscope", see Barna et al., Report No. SLAC-TN-72-3 (1972).

IV. RUNNING

The experiment can be divided into three running periods extending from Fall 1970 to Summer 1971. There were target and dump runs in each of these segments. The total amount of charge taken for each configuration is given in Table IV.

The timing of the event gate with the machine pulse was easy to achieve, as there was a large amount of sky shine (soft gamma rays) that came over the hill. We opened our apparatus to signals several hundred nanoseconds before the leading edge of the sky shine counts in our phototubes.

Using the counter near the dump and our counters we looked for the presence of any signals whose times-of-flight indicated particles whose speed was equal to or greater than that of light. There was no noticeable enhancement of the single counter rates during the early portion of machine pulses over a two-day period. If we assume that we were sensitive to the first 50 nsec of each pulse, we looked at about 0.1 coulomb in this manner.

The shielding was checked with a 20.8 GeV beam, the highest energy available. The singles rates in the counters showed no increase, so we concluded that there were no muons penetrating the shield. This energy is at least 1.3 GeV higher than any of the other running.

Total charge was measured by integrators attached to the toroids on the beam line. The figures for the second and third runs were measured to 0.1%, using the precision integrator in ESA, while those of the first were measured to 10%, using a more primitive integrator.

After each roll of film, approximately every eight hours, the experimental equipment was tested. Spark chamber efficiencies and counter rates were checked with cosmic rays. During the final run, the light diodes and calibration pulser allowed a complete check of the counters, logic, and superscope.

V. DATA REDUCTION AND ANALYSIS

Scanning Results

The spark chamber film was scanned for events that appeared to originate in the front three modules and be caused by a neutral particle travelling along the beam line. The film was scanned by physicists. Ten to fifteen percent of the pictures contained obvious cosmic rays. Almost all of the rest was blank, caused by sky shine accidental triggers. There were no other surprising event types.

There were single prong events in which there was one, usually straight, track and perhaps a few additional sparks at the origin (or end) point. These could have been tracks of cosmic ray muons entering from the downstream side and stopping in the chamber. The other possibility was neutrino events with a single muon or a muon and other particles not energetic enough to penetrate several aluminum plates. Several of the single prong events had very large bends and will be discussed later.

There were multiprong events with a common vertex. The numbers for each run are given in Table IV. All of these events had at least one possible muon candidate. We divided this group into the two prong events and the $\geq$ 3 prong events. The latter could be interpreted as highly inelastic neutrino events. There were a number of significant effects. They were consistent with the change in neutrino production caused by the different meson mean free paths in the various configurations. There also were two effects with likelihoods just below the 95% confidence level. There were fewer events, of any type, at lower energies. The two parts of the water target running gave different results, although there was no obvious physical

TABLE IV

Distribution of Events

Run	Configuration	Charge in Coulombs	2 Prongs	≥ 3 Prongs	≥ 3 Prongs / Total Multiprong	2 Prongs / Coulomb	3 Prongs / Coulomb	Single Prongs	Single Prongs / Coulomb
I	Water Dump 12-13 GeV	2.7	0	0		$0.^{+1.4}$	$0.^{+1.4}$		
	15 GeV	2.2	0	2	$1.0_{-0.8}$	$0.^{+1.7}$	$0.9^{+2.4}_{-0.8}$		
I - II	Water Dump 17-20 GeV	9.2	3	6	$0.7^{+0.2}_{-0.4}$	$0.3^{+0.6}_{-0.3}$	$0.7^{+0.8}_{-0.4}$		
III	Al Sphere Dump 19 GeV	13.1	4	2	$0.3^{+0.5}_{-0.3}$	$0.3^{+0.5}_{-0.2}$	$0.2^{+0.4}_{-0.1}$	8	$.6^{+0.6}_{-0.4}$
I - II	Water Target 19 GeV	2.6	8	2	$0.2^{+0.4}_{-0.2}$	$3.1^{+3.0}_{-1.8}$	$0.8^{+2.0}_{-0.7}$		
III	Water Target 19 GeV	6.3	8	11	$0.6^{+0.2}_{-0.3}$	$1.3^{+1.2}_{-0.7}$	$1.7^{+1.4}_{-0.9}$	13	$2.1^{+1.5}_{-1.0}$
	Water Target TOTAL	8.9	16	13	$0.4^{+0.2}_{-0.2}$	$1.8^{+1.1}_{-0.7}$	$1.5^{+1.0}_{-0.7}$		
II	Tantalum 19 GeV	4.7	2	1	$0.3^{+0.6}_{-0.3}$	$0.4^{+1.1}_{-0.4}$	$0.2^{+1.0}_{-0.2}$		

Note: Errors quoted for 95% confidence level on Poisson statistics.

reason for this. The surprising differences between the target and dump results after the first two runs were the main reasons why we continued the experiment. We now assume that these were statistical effects.

Several rolls of cosmic ray film, containing 4000 cosmic rays, were taken during the second run. This film contained 94 stopping muons of the type that can be confused with single prong neutrino events. It also contained a number of cosmic ray induced interactions which helped to explain some otherwise unusual events in the normal running.

Measuring

Vertex position and direction cosines were measured for all of the single and multiprong events. Direction cosines were also measured for a sample of 80 straight cosmic rays from the third run. The parameters for the transformation from the scanning table measurements to the laboratory were determined by the fiducial positions and the requirement that straight cosmic rays reconstruct to the counter that fired. Scanning table measurements were done to ± 1 mm which determined real space points to ± 0.5 inches horizontal and ± 3.5 inches vertical.

Superscope Calibration and Results

Time-of-flight calculations were done for all of the single prong events. The timing of the multiprong events was also checked for consistency with their interpretation as events caused by a particle that had penetrated the shield. The previously mentioned sample of cosmic rays was used for calibration.

Timing measurements were done in the following way. The beginning of each roll of film contained calibration shots. Each oscilloscope trace had two 8 nsec square waves at a known separation of ~ 30 nsec. This separation was found to be stable to within the measuring accuracy of 1 mm on the scanning table or 1.5 nsec. We measured the distance between the leading edge of a phototube signal and the leading edge of the calibration pulse associated with that half of the trace. The timing stability of the phototubes and light emitting diodes was verified by looking at the counter test pictures at the beginning of each roll. There was a barely noticeable jitter in these times, less than 2 nsec.

It remained to determine 42 - 1 additive constants for the 21 counters. There were two sets of constraints. For each counter, the difference of the two times should predict the correct position of a track along the length of that counter. Also, the time-of-flight of a particle between counters in different banks should be consistent with the observed distance and direction. A rough set of values for the first requirement was gotten by using the light emitting diodes. This was improved by imposing the requirement on the measured cosmic rays. The standard deviation of the difference between the measured times and the times predicted by the observed position was 2 nsec. This procedure failed for 5 of the 173 track-counter combinations. This could be due to the presence of a conflicting accidental signal not associated with a visible track. The second requirement was also imposed using the cosmic ray sample. We assumed that, since the tracks were straight, they were all travelling downward at the speed of light. At this point, we eliminated those tracks which appeared to be horizontal. Thus, we determined a track's direction of flight through the chambers and the spark chamber measurements gave the distance travelled between counters.

By repeated adjustment of the remaining 20 constants we reached a point were we could predict the direction of flight with 90% confidence. A track was said to be moving along the direction of the beam, if its time-of-flight was positive.

Separation of Single Prong Events

There were a total of 122 events with one track in the chambers. This mixture of single prong neutrino events and cosmic stopping muons could be separated using the particle's time-of-flight. We obtained the time-of-flight for 70% of these events. Failures were due to a lack of superscope information or a severe inconsistency for a single counter time difference. The bank-to-bank time difference between the two flight directions of a horizontal speed of light particle was at least 3.5 nsec. This BC combination occurred in only 13 of the 83 cases. Histograms of the particle time-of-flight for the third water target run and the aluminum dump run are given in Fig. 8. Zero time-of-flight, on this plot, corresponds to the case of a speed-of-light particle moving in the direction of the beam.

The single prong neutrino events show a symmetric distribution in the vertical angle. The horizontal and vertical angle distributions (Figs. 9 and 10) were similar for these events. The stopping muons, on the other hand, showed the expected asymmetric distributions in the vertical angle. The distribution of the stopping muon vertices showed a strong peak in the third chamber. This was not true for the neutrino events which only indicated an increasing trigger efficiency for downstream vertices.

The 39 events with insufficient timing information did not seem to have the characteristics of neutrino events. Most of them had end points in the

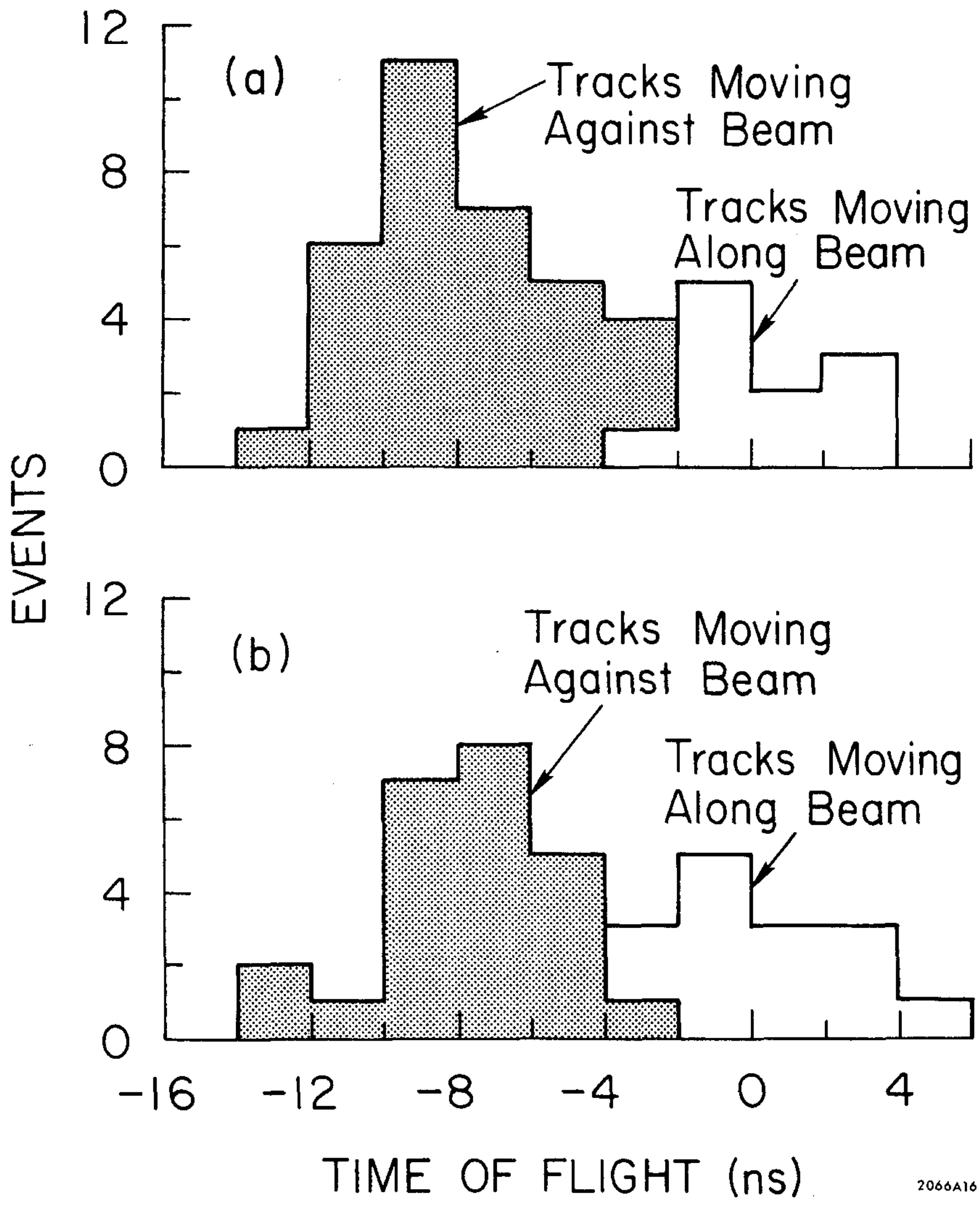

FIG. 8--Single prong time-of-flight. (a) Aluminum dump, (b) water target III.

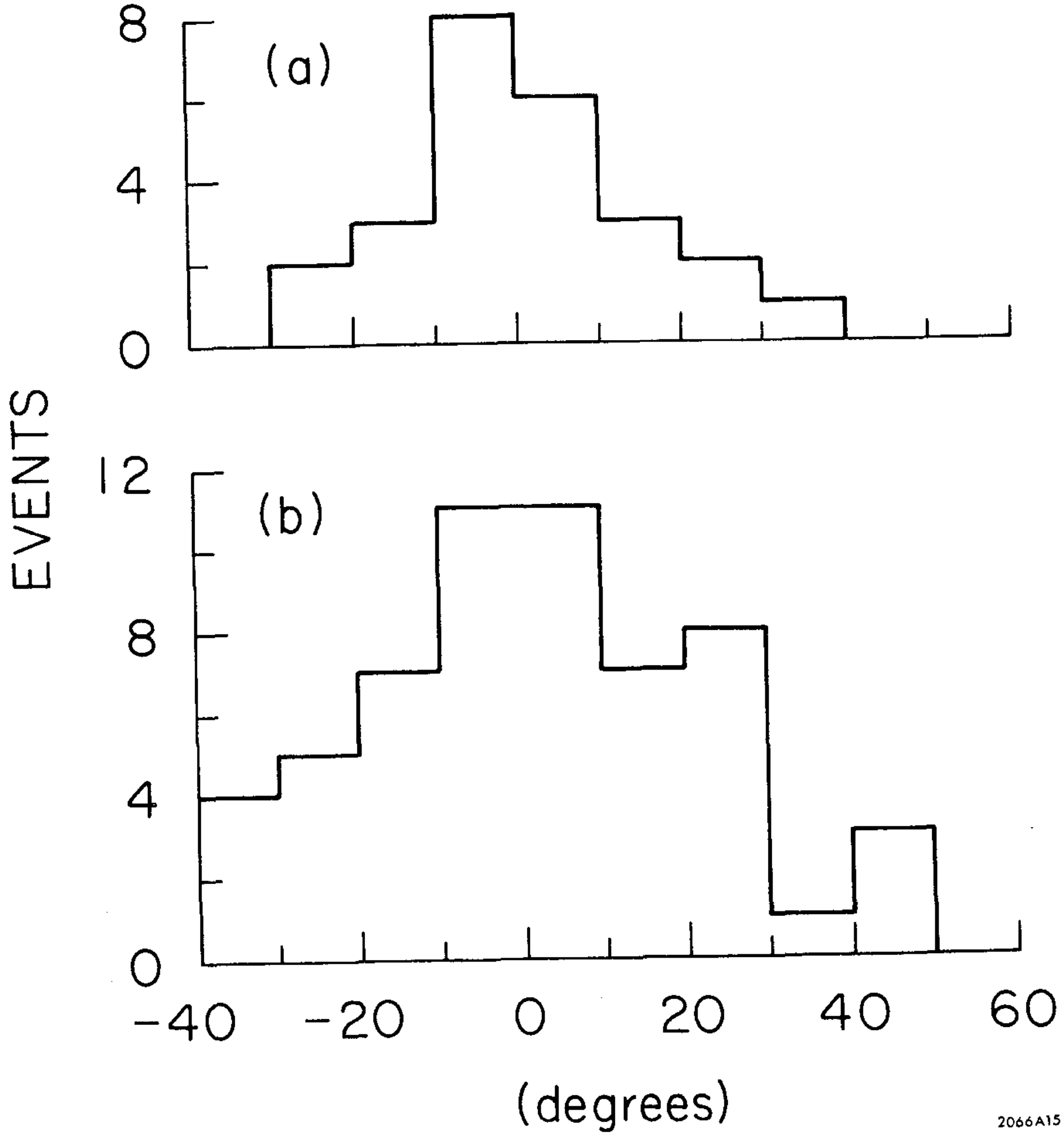

FIG. 9--Horizontal angle. (a) Tracks moving along beam, (b) tracks moving against beam.

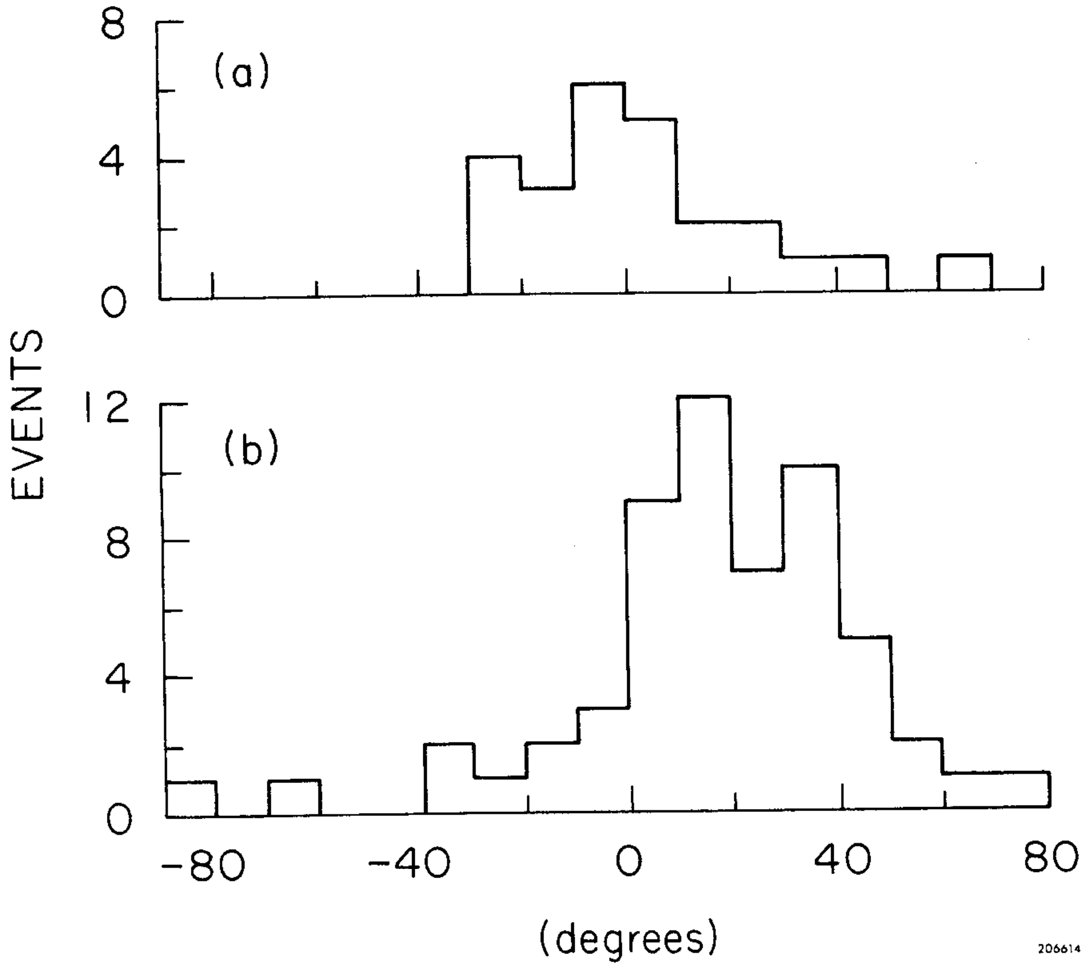

FIG. 10--Vertical angle. (a) Tracks moving along beam, (b) tracks moving against beam.

third chamber and very short tracks. Their direction cosines could not be determined very well. We concluded that they were mostly induced by cosmic rays and contained very few legitimate events.

The successfully analyzed group of events included 23 events with visible bends. Twenty of these analyzed as stopping muons. Most of the bend angles were $\sim 25^{\circ}$ but one of them was a right angle.

We corrected for our 90% direction choosing efficiency and got 12.8 ± 3.6 water target events and 8.3 ± 2.9 aluminum dump events for the final run. The errors quoted here are one standard deviation. Table IV shows the relation between the two runs. The ratio of the one prong rates between the water target and the aluminum dump runs was 3.5. The same ratios for two prong and ≥ 3 prong events were 4.3 and 8.5, respectively. Since the fraction of multiprong events increases with rising neutrino energy, we could see the trend of how the ratio of rates changed with energy.

VI. CALCULATION OF PARTICLE FLUX AND EVENT RATE

To understand the significance of our experimental results, we must be able to calculate our neutrino spectra in the target and dump runs, and the resulting event rates. For any theory which predicts unusual events, we must know what the expected event rate was as a function of the parameters, if any, of the theory. The elements of this calculation are the electron-photon cascade, which gave the gammas for photoproduction, the production of a particle, possibly followed by its decay into an interesting secondary, the geometry of our experiment, which determined part of the detection efficiency, and the interaction cross section and decay rate of the particle, which determined whether the particle would penetrate and be detected.

Electron-Photon Shower

The photons that produce the secondary particles discussed in Chapter II were produced by bremsstrahlung in our targets. We estimated the distribution of these photons as a function of energy and target thickness using formulas developed by Tsai.[20]

The shower was treated as the sum of successive generations of electrons and photons, each one generating the next generation of the other. The angular distributions were unimportant since the shower angle, $m_e/k \ll m_x/k$, for any of the secondary particles that we considered, and the angle subtended by our detector is also large compared to this angle. We used an approximation to the first generation photons;

$$I(t,k) = \frac{1}{k} \; \frac{(1-k/E_0)^{4t/3} - e^{-7t/9}}{\frac{7}{9} + \frac{4}{3}\,\ln(1-k/E_0)}$$

where E_0 is the incident electron energy, k is the photon energy, and t is the target thickness in radiation lengths. This formula was based on the calculation of the first generation electrons, with straggling due to the emission of bremsstrahlung, and, then, the first generation photons, with the absorption due to pair production. This result was good to 10% for the high energy half of the photon spectrum. Agreement to 15% was maintained for targets of up to 2.0 r.l. and $0.2 < k/E_0 < 1.0$, in spite of some numerical approximations. These comparisons were made to a more detailed calculation which retained the full first generation solution. The second generation photons would have given a contribution of < 10%.

This result was used to calculate secondary particle yields as follows;

$$Y = \frac{NX_0}{A} \int_0^T dt\, e^{-\eta (T-t)} \int_{k_{min}}^{E_0} I(t,k)\, \frac{d^2\sigma(k)}{dq d\Omega}\, dk$$

N = Avogadro's number

A = atomic weight of target nucleus

X_0 = unit radiation length in g/cm^2

η^{-1} = nuclear absorption coefficient (if any) per radiation length

T = total target thickness

$\frac{d^2\sigma}{dq d\Omega}$ = differential cross section for photoproduction

k_{min} = minimum photon energy for production process

which gives the yield per unit energy and solid angle of the secondary particles per incident electron. The integral over target thickness was trivial and we did it before we evaluated any particle yields numerically.

Calculation of Ordinary Neutrino Production

Neutrinos came from the decays of π and K mesons. We used an empirical production cross section[21] for these processes. This result was similar to Cocconi's phenomenological model[22] for proton induced secondary particles. It gave a better fit than the theoretical models to the experimentally observed yields.[23] Additional major contributions to both meson yields came from secondary π's and K's produced in π-N interactions. We used an empirical model,[24] similar to the one just mentioned, to calculate this contribution.

For pion production we took

$$\frac{d^2\sigma(k)}{dq\,d\Omega} = A^{2/3}\,\sigma_{\gamma p}\,2.2\,\frac{q^2}{\sqrt{k}}\,e^{\frac{-q}{1.1k^{3/4}}}\,e^{\frac{-q\theta}{0.2}}$$

where $\frac{d^2\sigma}{dq\,d\Omega}$ is the differential photoproduction cross section for a secondary particle with momentum q (GeV) at an angle θ. A is the atomic number of the target nucleus, $\sigma_{\gamma p}$ is the total γ-p absorption cross section and k is the photon energy. Kaon production was assumed to be given by the same formula, but reduced by a factor of 10. We assumed that the interaction cross sections are 45.3 $A^{2/3}$ mb for π's and 39.4 $A^{2/3}$ mb for K's. If we assumed that a particle was simply absorbed when it interacted, we got the results shown in Fig. 11. These were for a 0.3 r.l. beryllium target and an incident 18 GeV electron beam. The absorption parameter η is 0.84 for π's and 0.73 for K's. These yields are compared to the experimental results in Figs. 12 and 13. There was order of magnitude agreement between these yields and those calculated using the Drell process and the decay of the ρ meson (Fig. 14). Since we used targets with different atomic numbers, we

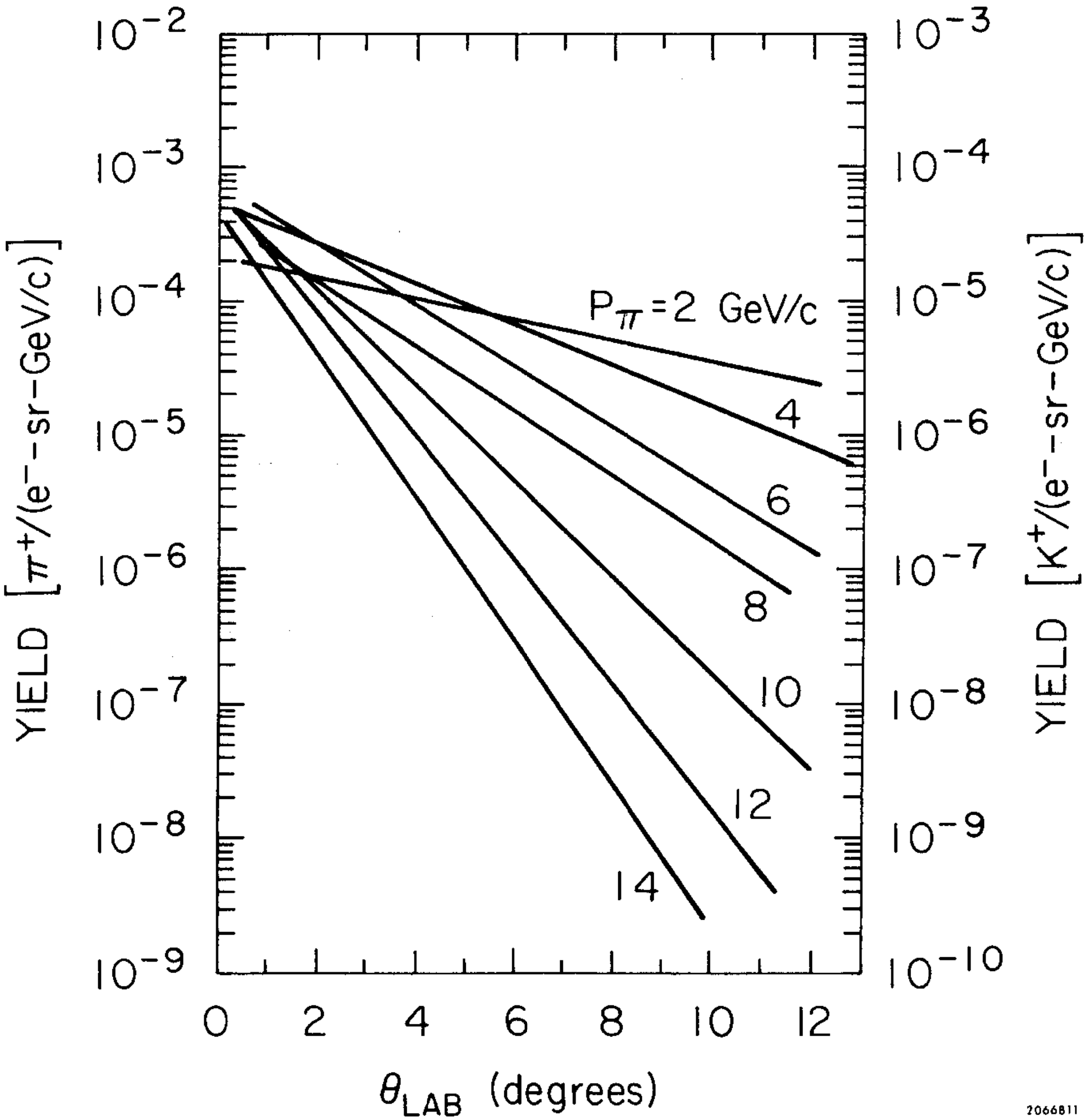

FIG. 11-- π and K yield, no interactions. 0.3 r.l. Be target, 18 GeV electrons.

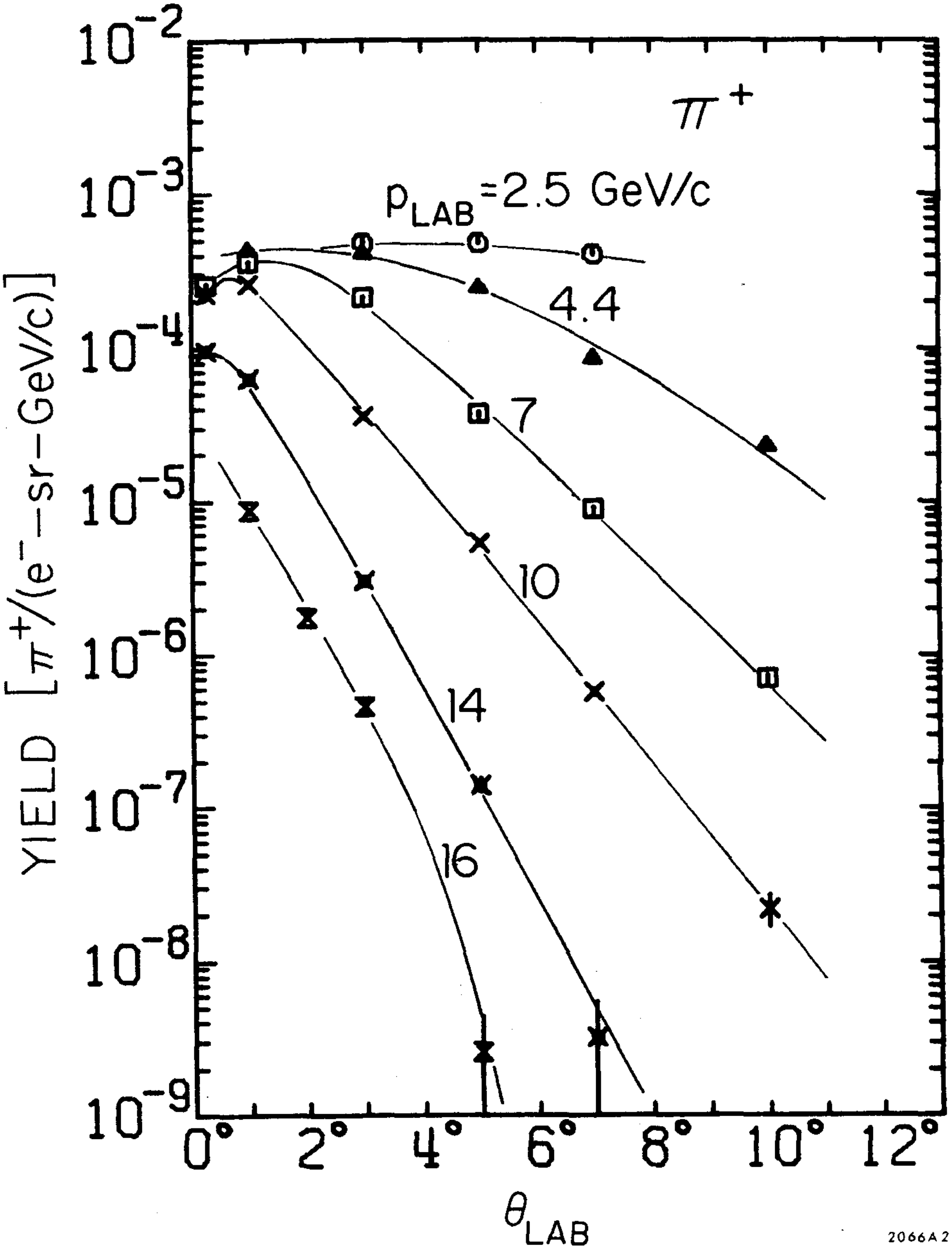

FIG. 12--Experimental π yields. Number of π^+ mesons from a 0.3 r.l. Be target per incident 18-GeV electron per unit solid angle per GeV/c. Only statistical errors are shown; in addition there are systematic uncertainties of $\pm 15\%$ when comparing yields at low and high momenta and $\pm 10\%$ in absolute normalization. The curves are merely shown to guide the eye.

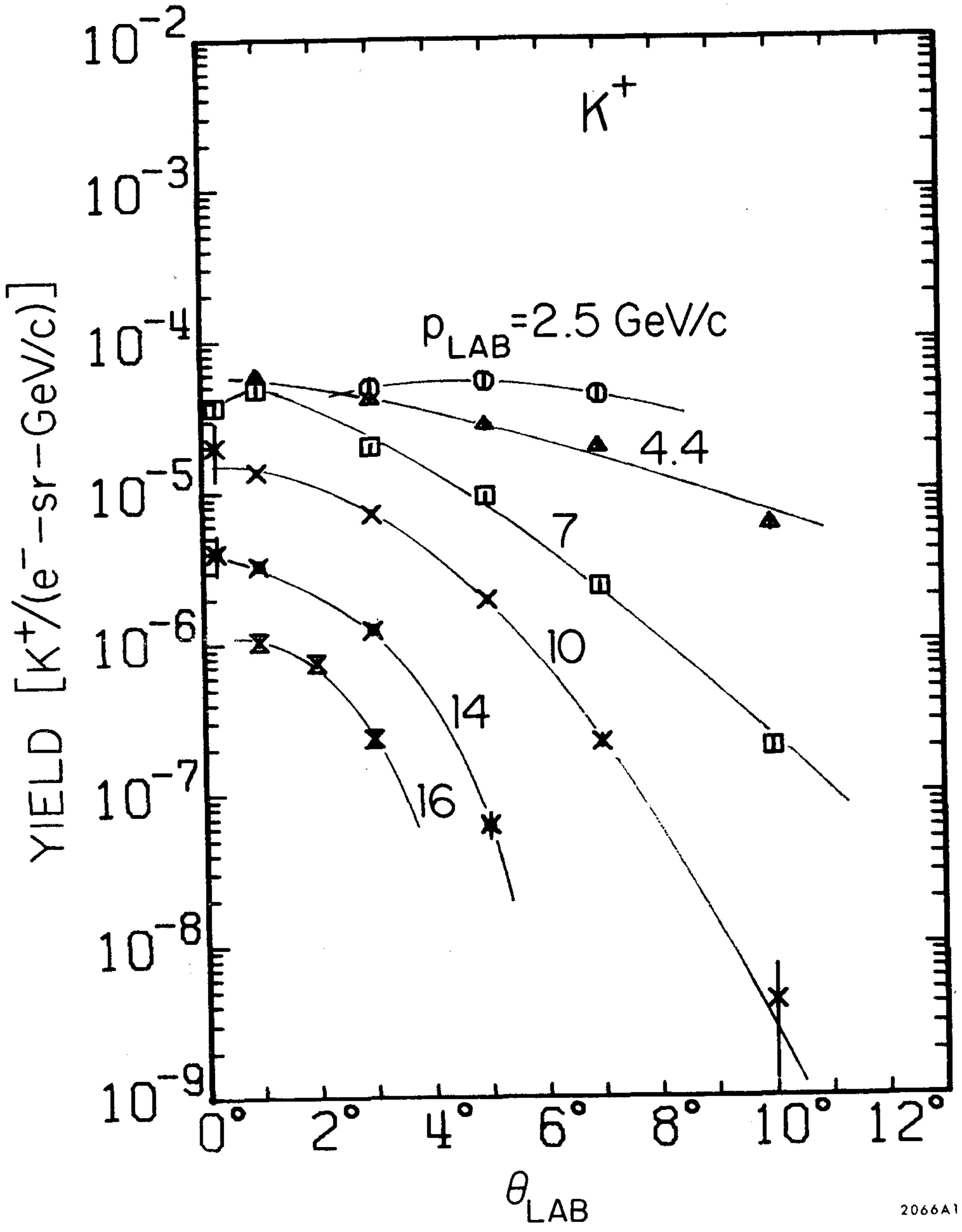

FIG. 13--Experimental K yields. Number of K^+ mesons from a 0.3 r.l. Be target per incident 18-GeV electron per unit solid angle per GeV/c. Only statistical errors are shown; in addition there are systematic uncertainties of ± 15% when comparing yields at low and high momenta and ± 10% in absolute normalization. The curves are merely shown to guide the eye.

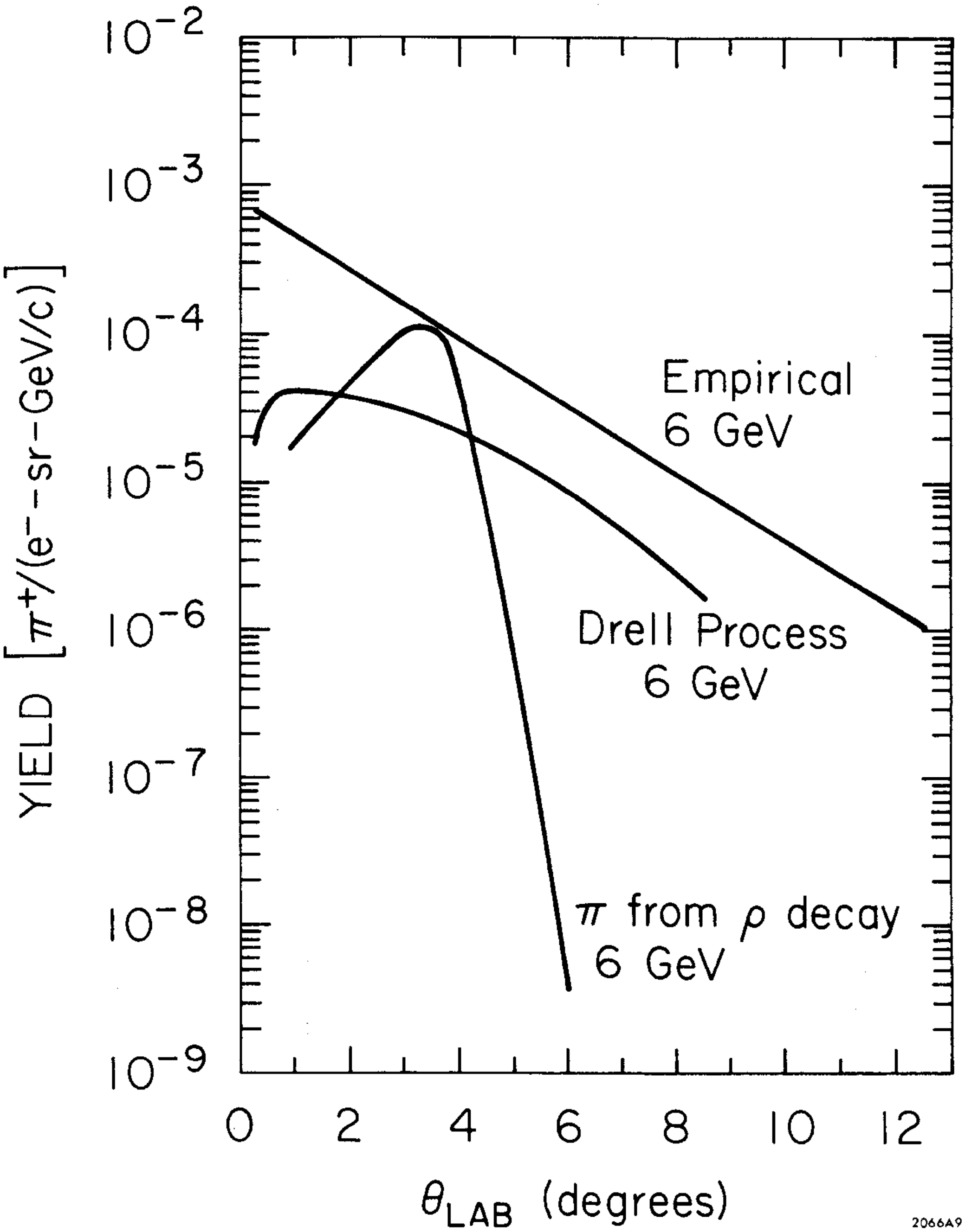

FIG. 14--Empirical, Drell process, and π by ρ yields.
0.3 r.l. Be target, 18 GeV electrons.

also wanted to look at the A dependence of these results (Fig. 15). We also needed the yield as a function of target thickness (Fig. 16). When absorption was included there was reasonable agreement between this model and the experimental results for 0.6 and 1.0 r.l. targets.

It can be immediately seen that we have underestimated the low energy yields. This showed us the importance of including secondary π's and K's. For the pion process, we took

$$\frac{d^2n(q)}{dp\,d\Omega'} = 6.4\, p^2\, e^{-3.76 \frac{p}{\sqrt{q}} - 4.23\, p \sqrt{q}\, \theta'^2}$$

$$+ 4.7 \frac{p^2}{q}\, e^{-10.2 \left(\frac{p}{q}\right)^2 - 4.3\, p\, \theta'}$$

where $\frac{d^2n}{dp d\Omega'}$ includes contributions from both π^+ and π^-, and θ' is the angle between the pions. The kaon production by pions was again down by a factor of 10. To use this result we needed to know the probability that an i^{th} generation pion would interact again. It can be seen from Fig. 16 that the yield increased almost linearly through most of a thick target. Therefore, we assumed that particles were produced at a constant rate in some fraction of the target. This meant that

$$n_i = \frac{1}{t_f} \int_0^{t_f} p_i(t)\, dt \qquad p_0 = 1$$

$$p_1 = 1 - e^{-(t_f - t)}$$

$$p_2 = 1 - e^{-(t_f - t)} - (t_f - t)\, e^{-(t_f - t)}, \ \ldots$$

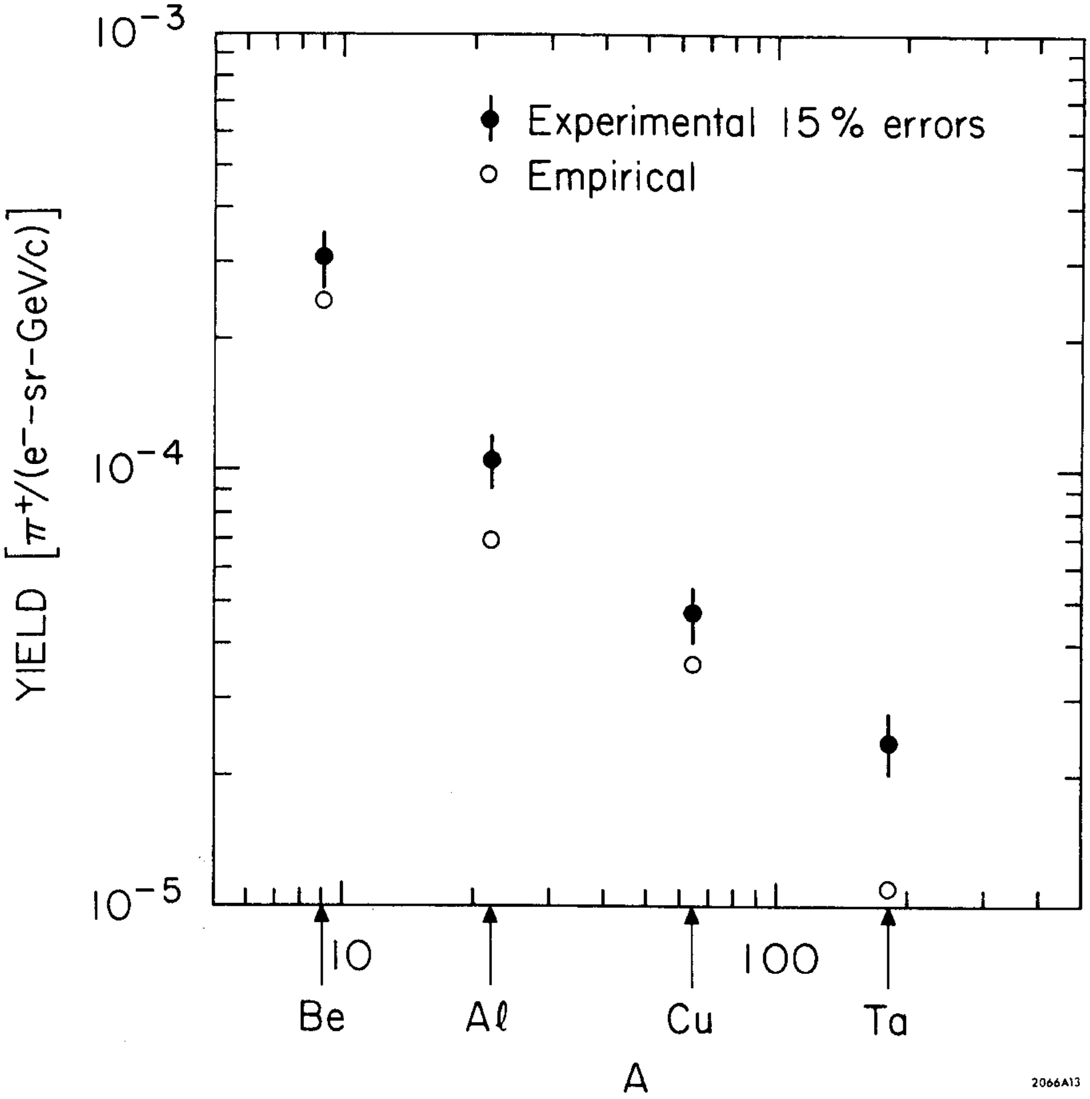

FIG. 15--A dependence of π yields. 0.3 r.l. targets, 18 GeV electrons, 7.0 GeV π's at 1^{o}.

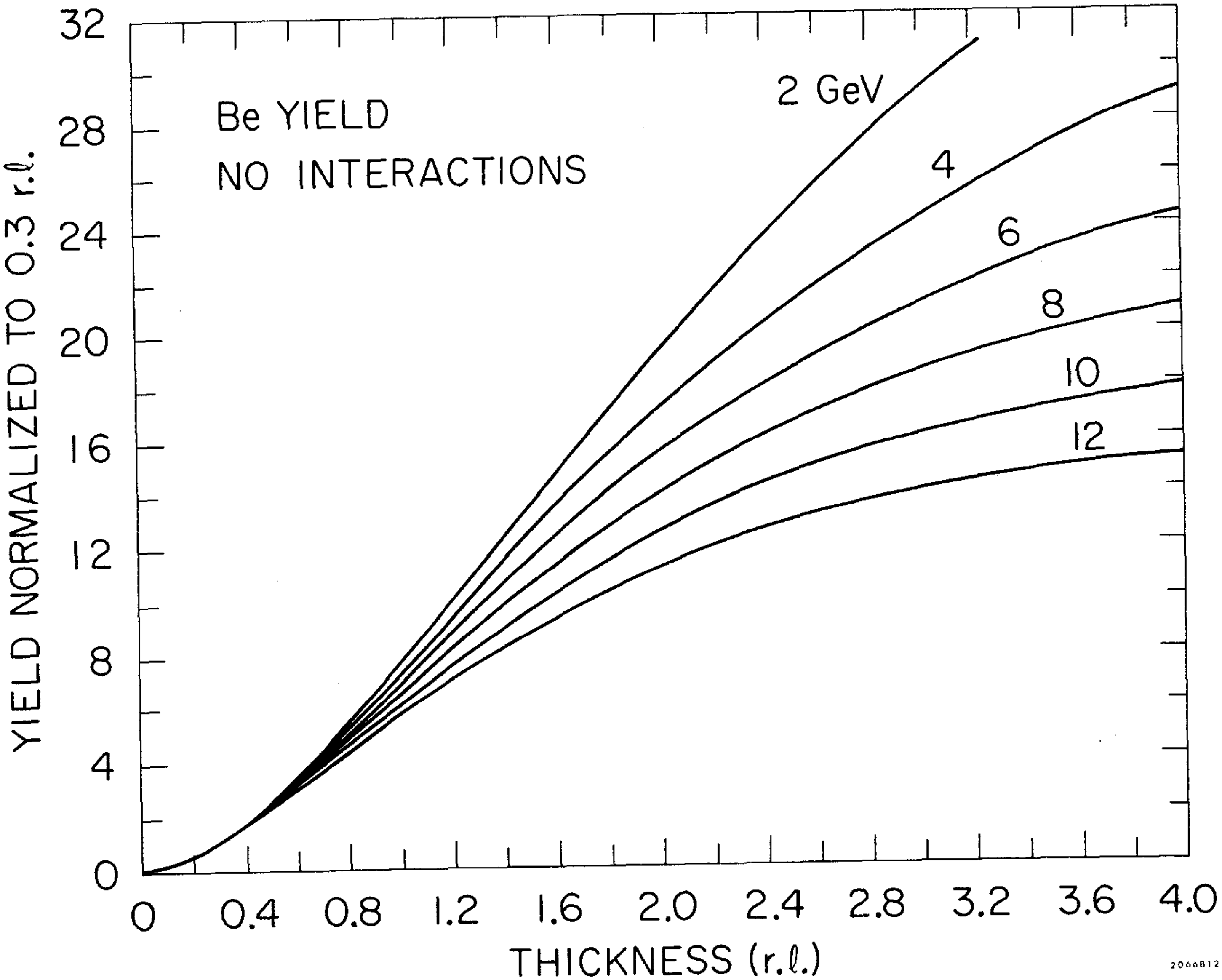

FIG. 16--Yield vs target thickness.

where n_i is the probability of a pion interacting i times, in a target of thickness t_f, measured in interaction lengths, and p_i is the corresponding probability density. Thus, n_{i+1}/n_i gave the probability that a pion made in the i^{th} generation would interact. We determined t_f from n_1/n_0, as calculated by the shower program with and without absorption.

We applied this procedure to the calculation of 0.3 r.l. Be yields. In this case, only the first generation of pion interactions was necessary. A numerical integration was done over the production and secondary angles, which are coupled, and the momenta, to give the final distribution as a function of the angle with the electron beam and the final momentum. The resulting pion yields (Fig. 17) are in considerably better agreement with the experimental points. When we applied this correction to the case of 1 r.l. Be, for 4 GeV pions at 3 degrees, we got a ratio of 8:1 over the 0.3 r.l. case. This was somewhat higher than the single experimental value of 6.5 : 1 and indicated that we may have overestimated the secondary yields for thick targets.

We could calculate the yield from an arbitrary target in the following way. Use the empirical procedure just discussed to calculate the ratio of yields between the arbitrary situation and the yield from a 0.3 r.l. Be target. Multiply by the experimentally measured yield from a 0.3 r.l. Be target. Hopefully, this procedure reduced the effect of any errors in our model.

We were then in a position to calculate the neutrino yield from the dump. The probability of decay was $\ell/(c\tau\gamma+\ell)$, where τ is the proper lifetime of the meson, γ is the time dilation factor and ℓ is the interaction length in the dump. All of the remaining mesons interacted. We did the additional integration over the production point analytically and then used the procedure

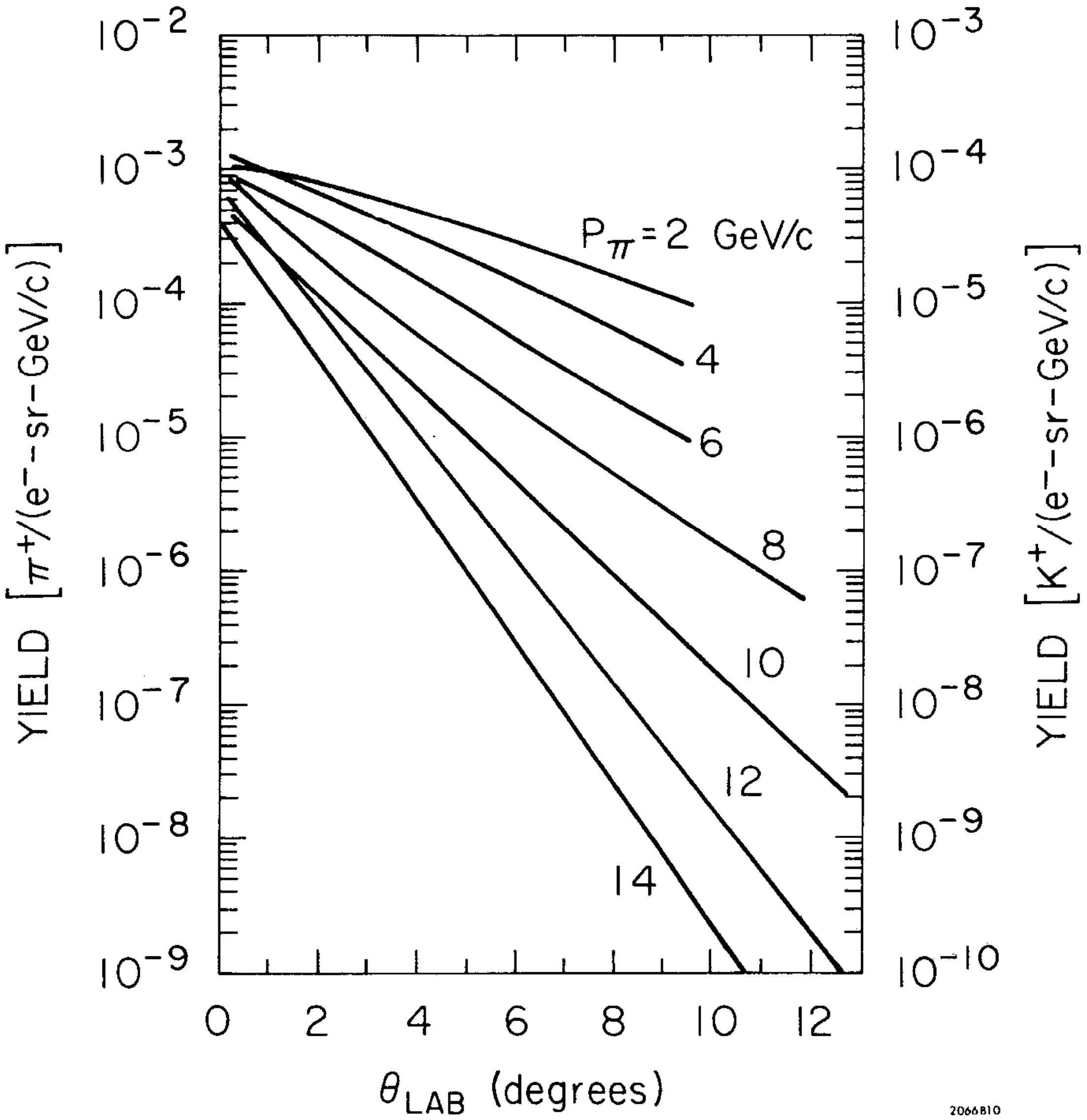

FIG. 17--π and K yields, with interactions.
0.3 r.l. Be target, 18 GeV electrons.

described above to calculate the yield of decaying mesons of a given energy and angle. Figure 18 shows the decaying π yield at 1° as a function of π momentum and electron energy. We now have the explanation for the experimental trend in the event rate as a function of beam energy. A simple Monte Carlo program calculated the neutrino spectrum at the detector by folding together the production spectrum, the kinematics of the meson decays, and the geometry of the apparatus.

The calculation of the neutrino yield from the target configuration was similar. The contributions to the yield were from the decays of mesons produced in the target and also from the decays of mesons produced by the remaining portion of the shower as it hit the dump. The latter case was just discussed. For the target case, we first calculated the production of the mesons. A generalization of the Monte Carlo program simulated the decays occurring in the pipe between the target and the dump, and gave the neutrino spectrum at the detector.

The calculated neutrino spectrum at the detector was converted into an event rate. We assumed a total neutrino cross section of 0.8×10^{-38} E cm^2/nucleon. We also estimated the triggering efficiency of our third run detector. Figure 19 shows the results of a Monte Carlo calculation of the geometric trigger efficiency as a function of the angle of an emitted charged particle from a neutral event. We obtained the overall detection efficiency by combining this result with the observed angular distribution of our single prong neutrino events.

The ratio of the event rates from the water target and the aluminum dump should be independent of many of the detailed characteristics of the model used. We obtained a value of 1.3 : 1. If we required that the neutrino energy

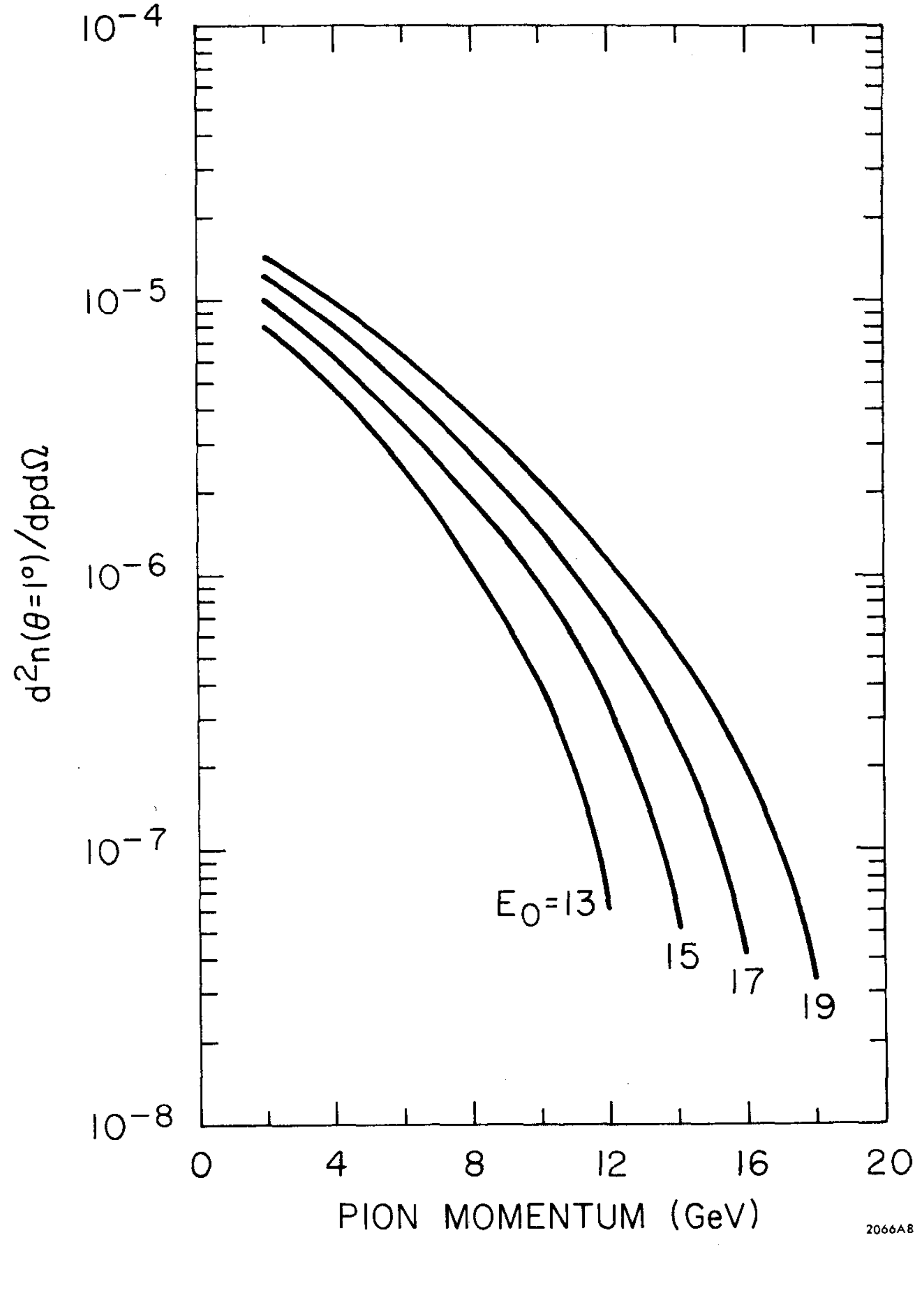

FIG. 18--π decay yield vs π momentum and incident electron energy. Aluminum sphere dump.

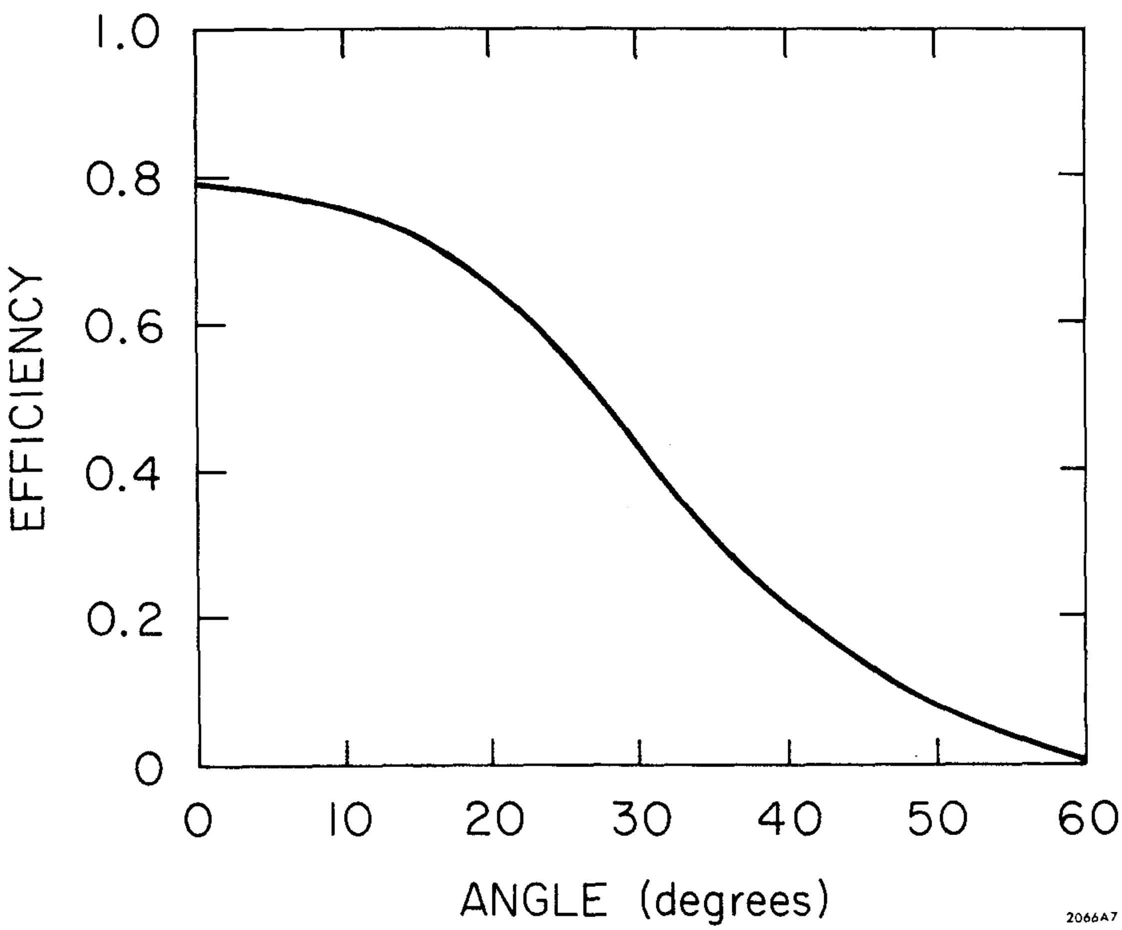

FIG. 19--Geometric triggering efficiency.

be above 1 GeV this became 2.1 : 1. If we looked at a 3.5 GeV neutrino energy we got 4.5 : 1. If we excluded the contributions of mesons under 2 GeV, the region where we probably have the largest overestimate of interaction production, we got 4.5 : 1. The other obvious error in the calculation was omitting the effects of pions hitting the vacuum pipe between the target and the dump, which would also have raised the ratio. Our calculation gave approximately the same trend of the ratio as a function of energy as was observed experimentally.

The prediction of the event rate itself was much less certain. We calculated 10.0 events/coul in the water target mode. This number was reduced by a factor of 2.0 if we demanded that the neutrino energy be above 1 GeV. The experimental result was 5.1 ± 0.9 events/coul. In the aluminum dump mode, the calculation gave 7.5 events/coul or 2.1 events/coul for $E_\nu > 1$ GeV. Here, the experimental result was 1.1 ± 0.3 events/coul. The prediction of the event rate for the water dump was larger. There is a factor of $\ell_{H_2O}/\ell_{Al} = 1.4$, since the decay in water is more likely, and a factor of $A_{Al}/A_{H_2O} = 1.7$ since the production went roughly as $1/A$. The event rate in the water dump was higher, but numerical comparisons would be futile because of the low statistics. Similarly, the yield from the tantalum run should have been depressed, from that of the aluminum, by a factor of ~ 13 at high energy. The low energy mesons would not have been as strongly suppressed, since only 3.0 r.l. of tantalum were used.

It is interesting to compare our neutrino spectrum (Fig. 20) with that of a proton accelerator (Fig. 21). We used the spectrum of the second Brookhaven experiment[18] and our water target spectrum. The shapes are similar, but in our case, the neutrinos from K's dominated above 1.7 GeV.

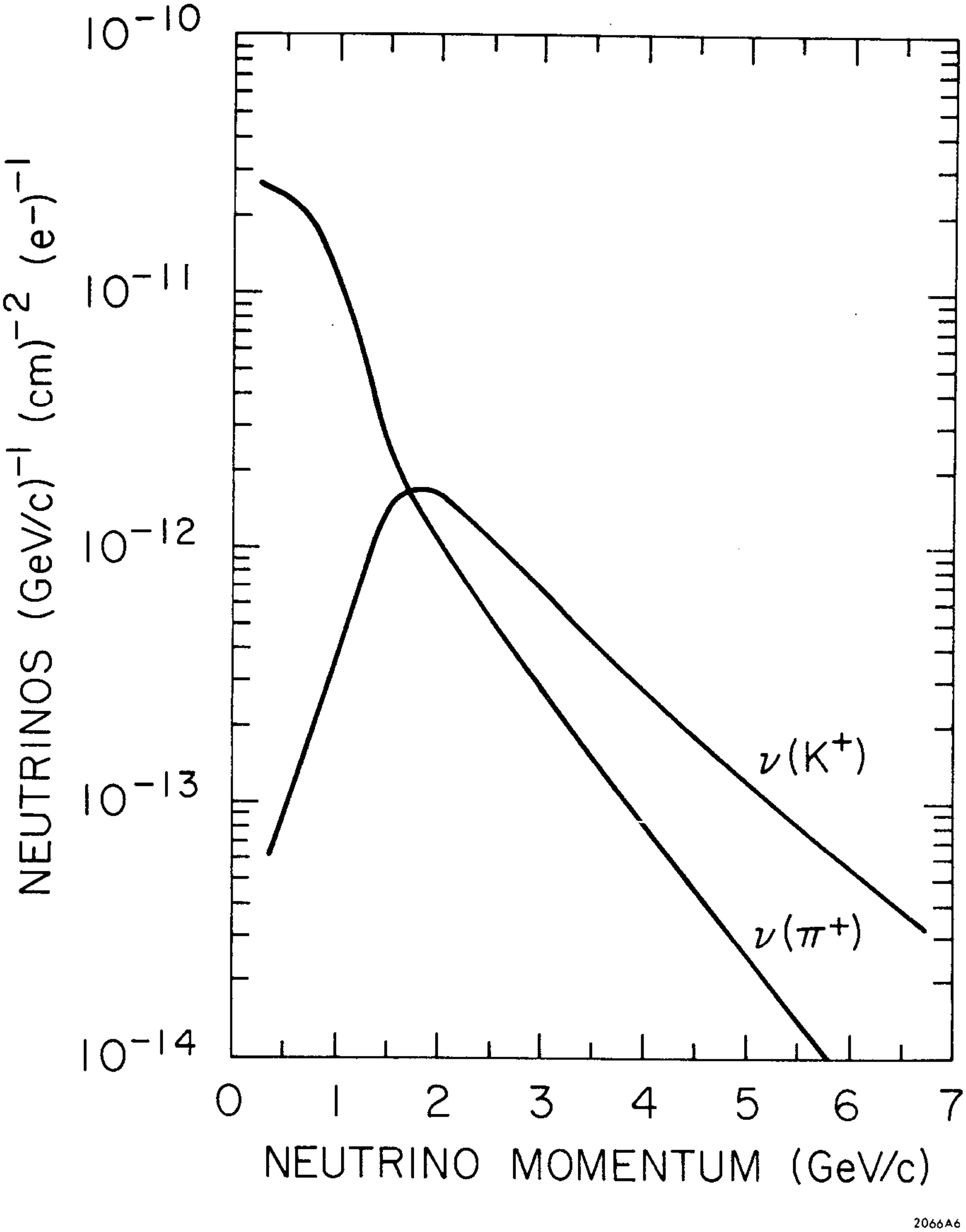

FIG. 20--Neutrino spectrum, water target configuration.

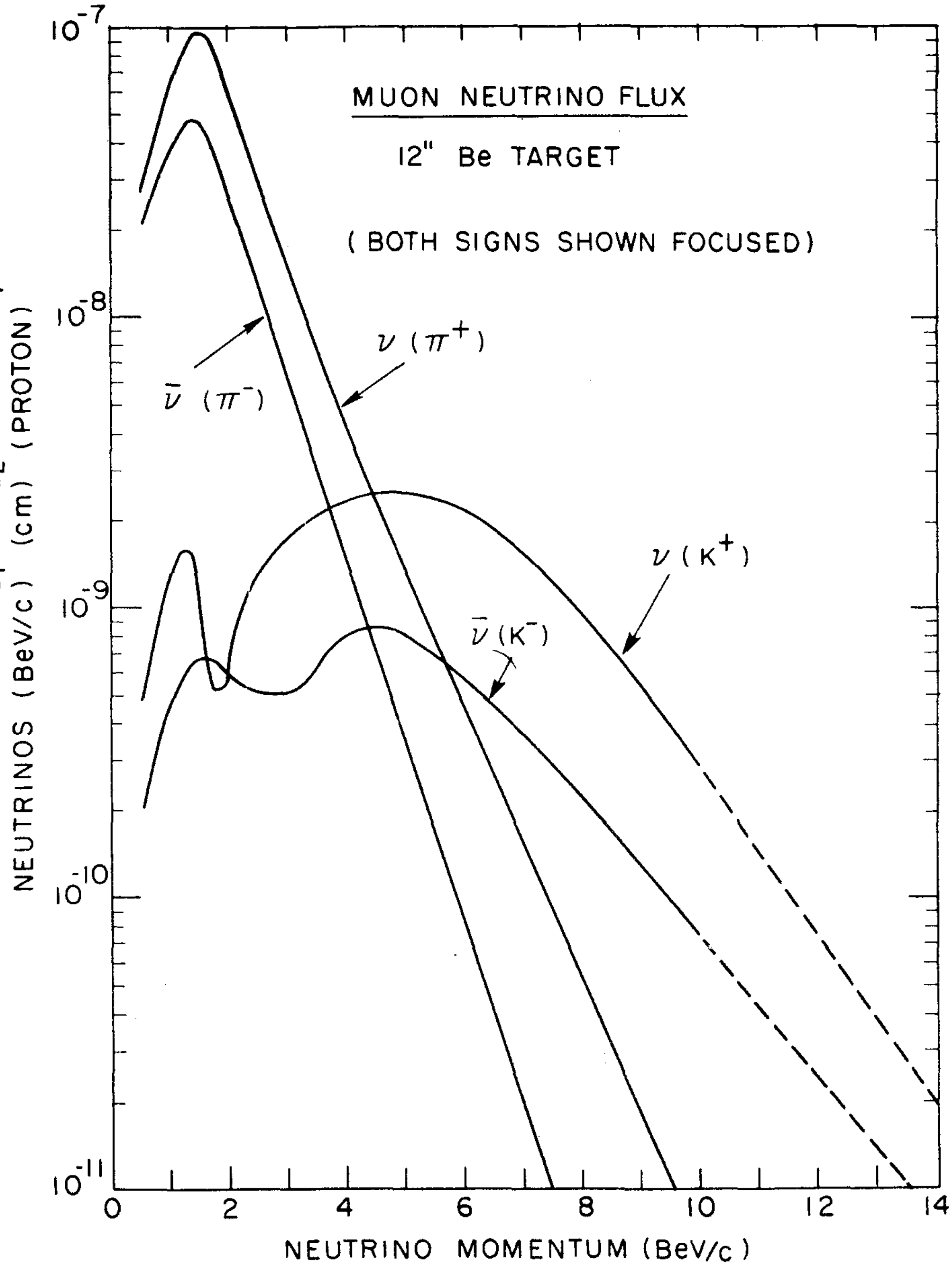

FIG. 21--Neutrino spectrum at Brookhaven, using a focusing device.

The Brookhaven experiment used a magnetic focusing device. At an electron machine, focusing is mimicked by the small angles, $\sim m_\pi/E_\pi$ in the production process. A major difference is that we had nearly equal fluxes of neutrinos and antineutrinos, while a magnetic focuser selects one or the other. Another major difference was a factor of 6 in the solid angle, since a 75 ft steel shield was used at Brookhaven. The scales on these two figures are roughly equivalent, 10^{11} proton/sec at Brookhaven and 10^{14} electron/sec at SLAC. For our water target mode the ratio of single prong events to all events was 0.4 ± 0.2, as compared to $\sim 1/2$ at Brookhaven.

Calculation of Heavy Lepton Neutrinos

The production and decay of a photoproduced heavy lepton was discussed in Chapter II. We need only combine these effects with the shower and the geometry of our apparatus to get the flux of heavy lepton neutrinos at our detector. To get the event rate, we assumed that the total cross section, above threshold, was given by the same, linearly rising, formula as was used for muon neutrinos. The signature of a heavy lepton neutrino event would have been distinctive in that there was a low probability of a muon appearing as a decay product.

We used the production formula in the shower program to get the heavy lepton yield as a function of energy and angle in the aluminum dump. To get the neutrino flux, we did a numerical integration.

$$\frac{d^2n}{dk\,d\Omega''} = \int \frac{d^2n(\theta, p; E_0)}{dp\,d\Omega} \frac{d^2n(\theta', k; p)}{dk\,d\Omega'} \, d\Omega \, dp$$

where $\cos\theta' = \cos\theta \cos\theta'' - \sin\theta'' \sin\theta \cos\phi$

$\frac{d^2 n(\theta, p; E_0)}{dp d\Omega}$ = differential yield of heavy leptons of momentum p from an electron beam of energy E_0 and at an angle θ to that beam

$\frac{d^2 n(\theta', k; p)}{dk d\Omega}$ = differential decay yield for the decay of a heavy lepton of momentum p giving a neutrino of momentum k at an angle θ' to the lepton

$\frac{d^2 n}{dk d\Omega''}$ = differential yield of heavy lepton neutrinos of momentum k at an angle θ'' with respect to the electron beam.

This assumed that the heavy lepton decays rapidly without losing much energy or traveling a significant distance away from the beam line. The resulting heavy lepton neutrino event rate as a function of lepton mass is given in Fig. 22. The contribution to the rate comes from high energy neutrinos, ~ 5 GeV for a 0.5 GeV heavy lepton. If we demand a 5 event signal in the aluminum dump run, we get a mass cutoff of 0.4 GeV. Thus, we can make the statement that we saw no evidence for heavy leptons with a mass below 0.4 GeV. Of course, this statement has already been made, since K's are not observed to decay into heavy leptons. A more interesting conclusion could have been reached if we had had a better solid angle. Improving the solid angle by a factor of 10 would allow us to set a mass limit of 0.6 GeV.

We also calculated the contribution to the ordinary neutrino flux from muons using the heavy lepton production program to calculate the muon

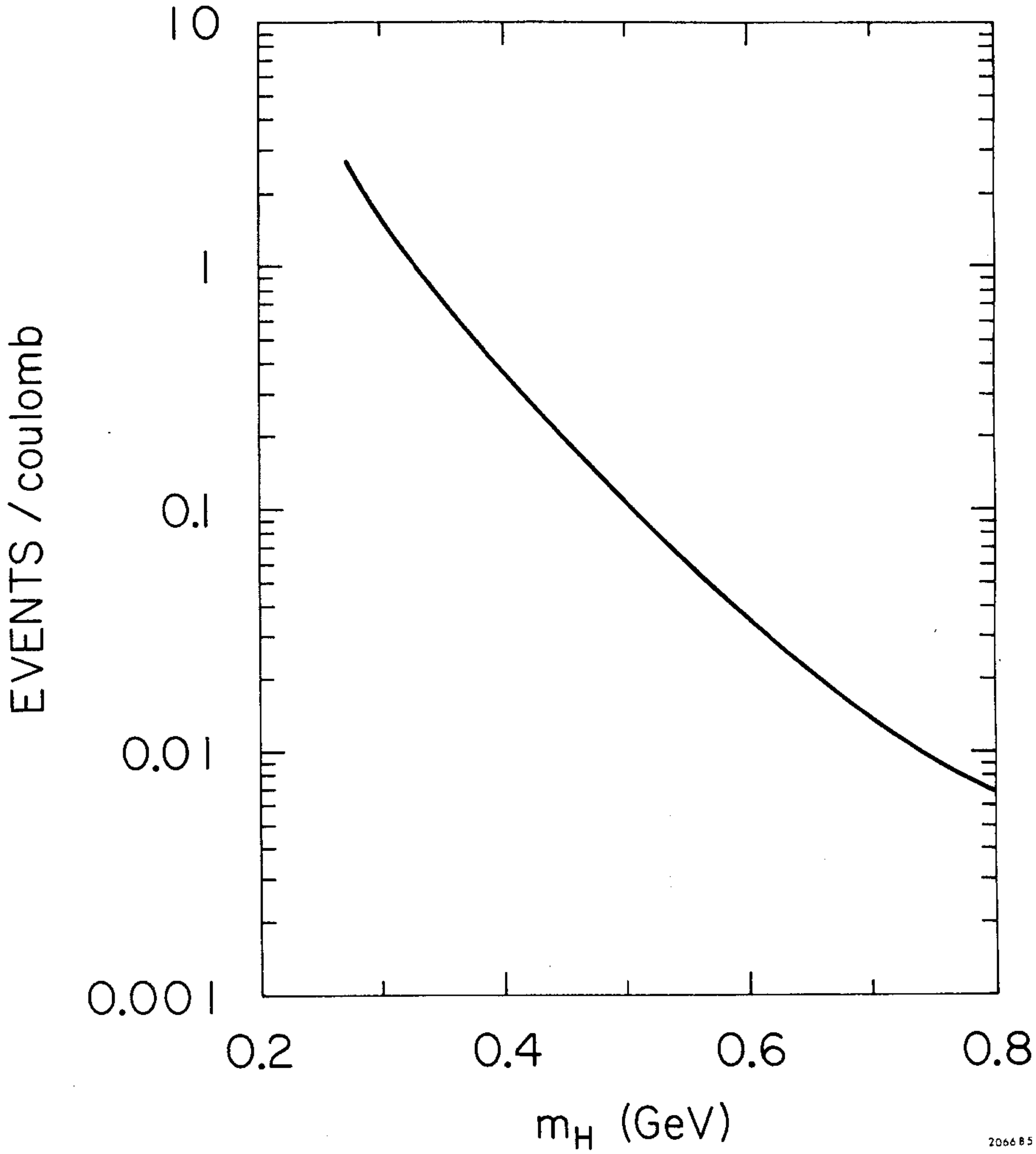

FIG. 22--Heavy lepton neutrino event rate.

yields. In treating the muon decay, we had to consider the lifetime and the energy lost by the muon in the shield. The resulting neutrino spectrum was negligible compared to the contribution from pions and kaons.

Generalized Limit on Unknown Processes

We are now in a position to set a general, order of magnitude, limit on the production and interaction of a particle that could penetrate the shield. This can be conveniently expressed as a limit on the product $\sigma_{prod} f_{\Omega} \sigma_{int} f_{tr}$, where σ_{prod} is the production cross section on a single proton (thus removing the nuclear effects), f_{Ω} is the ratio of the production solid angle to our detector's solid angle, σ_{int} is the interaction cross section per nucleon, and f_{tr} is the probability of transmission through the shield. If we assume that $\sigma_{int}(A) = A^{2/3}\, \sigma_{int}$ and that this is the only mechanism at work, we get $f_{tr} = e^{-2.7\times10^{27}\, \sigma_{int}}$. We can use the case of the 0.5 GeV heavy lepton to evaluate the product. The single proton production cross section is 1.6×10^{-33} cm^2. The lepton yield and the neutrino yield are roughly the same. The solid angle factor is 0.2. The interaction cross section is 3×10^{-38} cm^2 and absorption is negligible. We would like to see an additional factor of ~ 10 in the event rate to be sure we have a signal. Combining this, we get a limit of $\sigma_{prod} f_{\Omega} \sigma_{int} f_{tr} > 10^{-70}$ cm^4 for our apparatus to detect events. Figure 23 gives a plot of this relation, using the previously mentioned assumption about f_{tr}.

For the case in which we want to observe a particle decaying in the gap between the chambers, we must replace σ_{int} by $e^{-6.5\times10^{3}/\gamma c\tau}\ 2.2\times10^{-24}/\gamma c\tau$ where the first factor comes from decays in the shield and the second comes from the ratio of the probabilities of interacting in the chamber or decaying

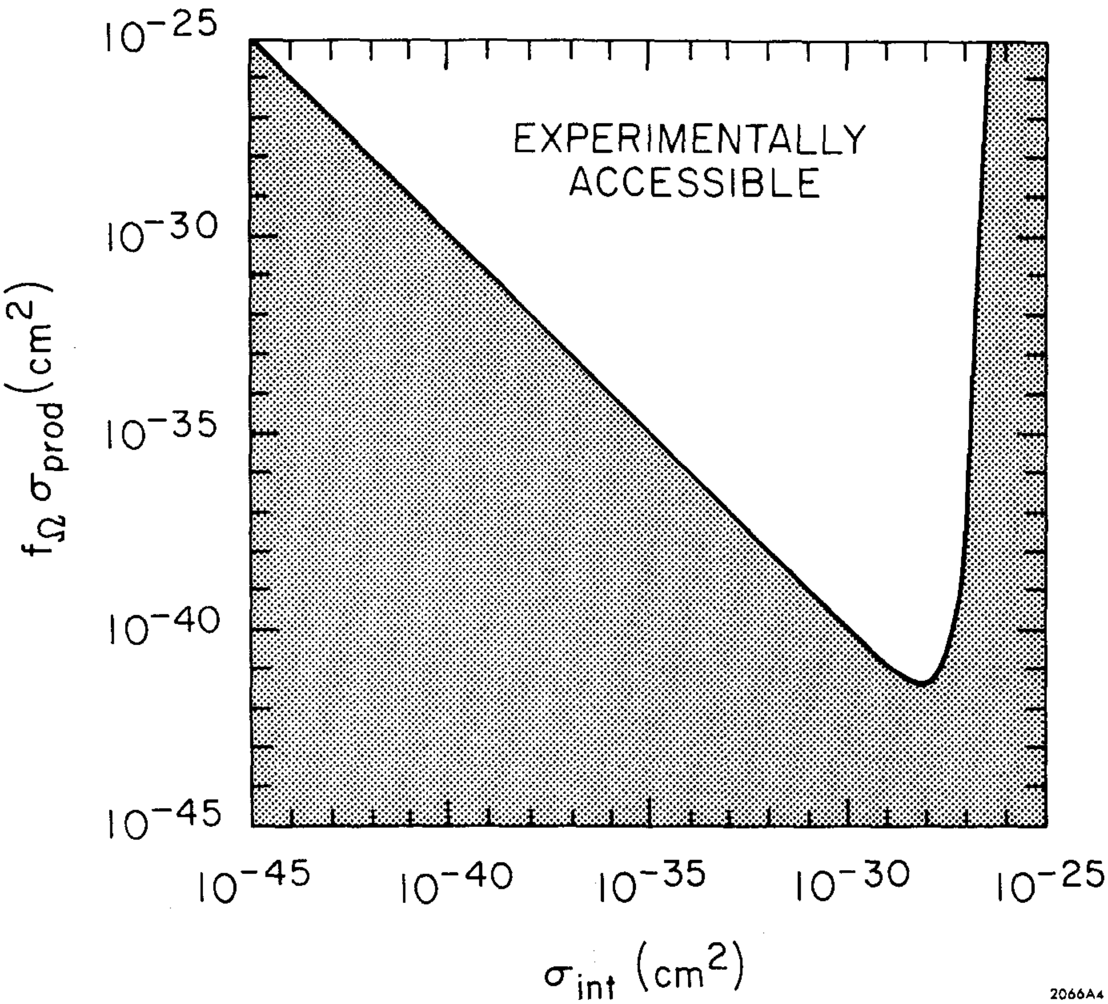

FIG. 23--Generalized limit on production and interaction of penetrating particles.

in the gap. This means $\gamma c\tau \; e^{6.5\times 10^{3}\,\mathrm{cm}/\gamma c\tau} < 2.2\times 10^{46}\ \mathrm{cm}^{-1}\ \sigma_{\mathrm{prod}} f_{\Omega} f_{\mathrm{tr}}$ for decays to be seen in our apparatus (Fig. 24).

We can examine the experimental evidence against the long range interaction model proposed in Chapter II. We insert the production and detection cross sections previously mentioned into our expression for the sensitivity of our experiment. The cross sections are too small for absorption to have a significant effect. We get the following order of magnitude limits for the observation of "light": $(\alpha'/\alpha)^2/m_A^6 > 3\ \mathrm{GeV}^{-6}$ for the A not interacting strongly, $(\alpha'/\alpha)^2/m_A^6 > 10^{-4}\ \mathrm{GeV}^{-6}$ for strongly interacting A, by the coupling constant argument. The limits that we get using $\sigma_{\gamma p \to A + \text{anything}}$ are considerably stronger. For the K, we would see the "light" if $\alpha'/\alpha > 3 \times 10^{-5}$ and for the A2 we would see events if $\alpha'/\alpha > 10^{-3}$. Thus, we find no evidence of an interaction between strange particles similar to the electromagnetic interaction between charged particles.

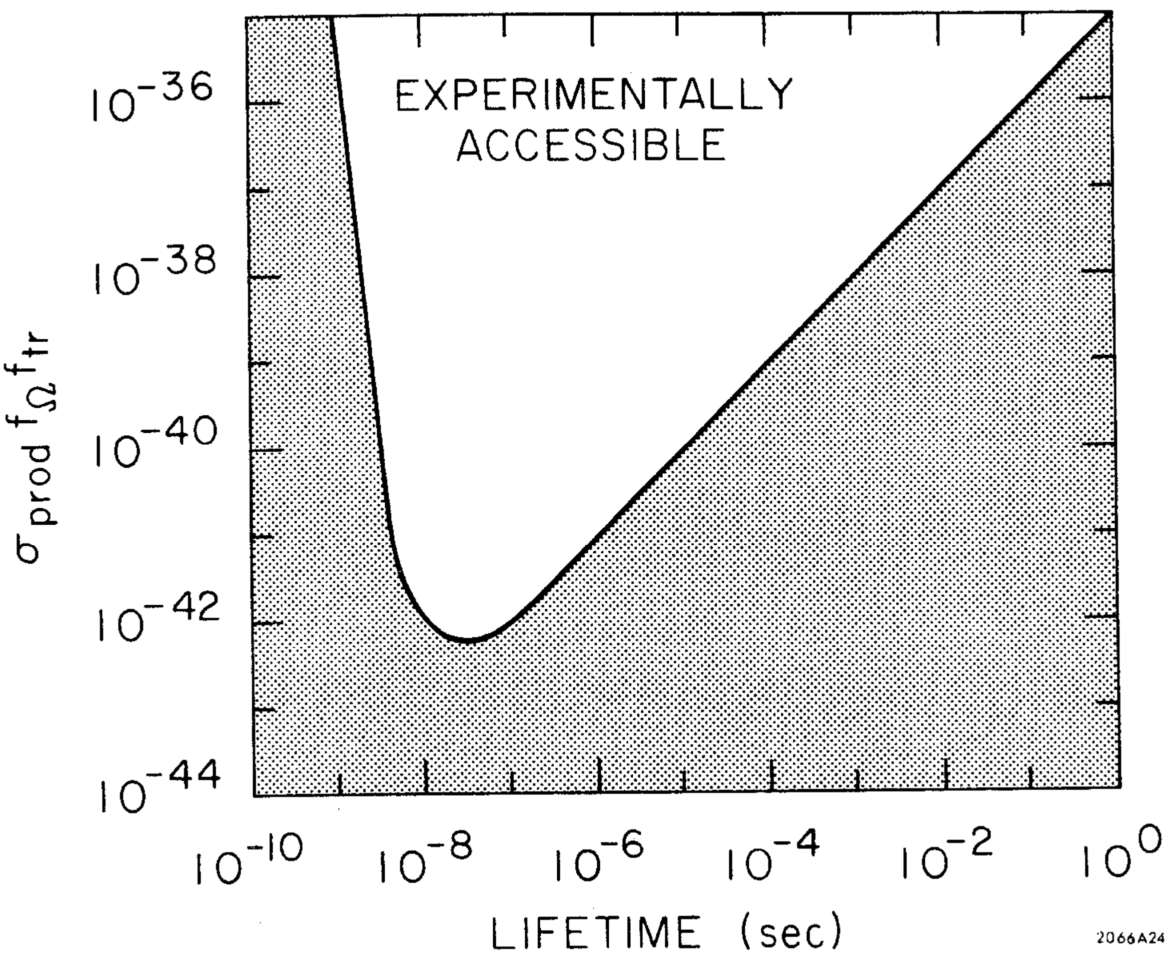

FIG. 24--Generalized limit on production and detection by decay of penetrating particles. $\gamma = 10$.

VII. CONCLUSIONS

We have conducted an experiment to look for new penetrating particles and to look for possible differences in neutrino production at an electron accelerator as compared to a proton accelerator. There was no evidence for either effect.

We observed ~ 100 neutrino events in several different production configurations. The events rates were consistent with the interpretation that the neutrinos came from the decays of π and K mesons produced in the targets. The changes in these rates agreed with the changes predicted knowing the composition of the targets and the mesons' mean free paths. The ratio of elastic to inelastic neutrino events agreed with the ratio observed at the proton accelerators.

The experiment did not have sufficient sensitivity to make any interesting statement about the existence of heavy leptons of mass greater than that of the K. However, the same experiment could still be done with an improved solid angle and it would make such a statement. The solid angle could be increased by using an iron instead of an earth shield.

We set a limit on any unknown source of penetrating particles that would interact in our detector:

$$\sigma_{prod} f_{\Omega} \sigma_{int} f_{tr} < 10^{-70} \text{ cm}^4,$$

where σ_{prod} is the production cross section on a single proton, f_{Ω} is the ratio of the production solid angle to our detector's solid angle ($\approx 3 \times 10^{-3}$ sr), σ_{int} is the detectable interaction cross section per nucleon, and f_{tr} is the probability of transmission through the shield. We also set a similar limit on any unknown source of a massive penetrating particle with a finite lifetime, $\gamma c \tau \; e^{6.5\times 10^{3}\ \mathrm{cm}/\gamma c\tau} > 2.2\times 10^{46}\ \mathrm{cm}^{-1}\, \sigma_{\mathrm{prod}} f_{\Omega} f_{\mathrm{tr}}$.

REFERENCES

1. Reviews of the current experimental and theoretical situation can be found in: C. H. Llewellyn Smith, "Neutrino Interactions at Accelerator Energies," Report No. SLAC-PUB-958 (May 1971)(to be published in Physics Reports). Informal Conference on Experimental Neutrino Physics, Report No. CERN 65-32 (December 1965). Neutrino Meeting, Report No. CERN 69-20 (November 1969).
2. Panofsky, Newton, and Yodh, Phys. Rev. 98, 751 (1955).
3. Kim and Tsai, "An Improved Weizsacker Williams Method and Photo-Production of Lepton Pairs," Report No. SLAC-PUB-1030 (1972) (submitted to Physics Letters).
4. Drell and Walecka, Ann. Phys. 28, 18 (1964).
5. Drell, Phys. Rev. Letters 5, 278 (1960).
6. Tsai, "Estimates of Secondary Beam Yields at SLAC," SLAC User's Handbook (1968).
7. Rosenberg, Phys. Rev. 129, 2786 (1961).
8. Bernstein, Ruderman, and Feinberg, Phys. Rev. 132, 1227 (1963).
9. Rothe and Wolsky, Nucl. Phys. B10, 241 (1969).
   Gershstein and Folomeshkin, Soviet J. Nucl. Phys. 8, 447 (1969).
10. Barna *et al.*, Phys. Rev. 173, 1391 (1968).
    Alles-Borelli *et al.*, Lett. Nuovo Cimento 4, 1156 (1970).
11. Schwartz, "A Proposed Method to Search for Intermediate Bosons and Heavy Leptons," Report No. SLAC-5 (1962) p. 29.
12. Tsai, Phys. Rev. D4, 2821 (1971).
13. Schwartz (private discussion).

14. Bethe and Rohrlich, Phys. Rev. 86, 10 (1952).
Rohrlich and Gluckstern, Phys. Rev. 86, 1 (1952).

15. G. Antonnen, "A Mechanical Analysis of Miocene Sandstones from the SLAC Site," Stanford University (June 1966)(unpublished).

16. Galbraith et al., "Absorption Cross Sections for High Energy Protons, Antiprotons and Pi and K Mesons on Nuclei," Report No. BNL-11598 (1966).

17. High Energy Particle Data. Volume IV, Range, Momentum and dP/dx Plots of Charged Particles in Matter. Report No. UCRL-2426 (1966).

18. Burns et al., Phys. Rev. Letters 15, 42 (1965).
Burns, Nevis Report No. 148, Ph.D. Thesis, Columbia University (1966). Rettberg, Nevis Report No. 152, Ph.D. Thesis, Columbia University (1966). Hyman, Nevis Report No. 158, Ph.D. Thesis, Columbia University (1967).

19. Dorfan et al., Phys. Rev. Letters 19, 987 (1967).

20. Y. S. Tsai and Van Whittis, Phys. Rev. 149, 1248 (1966).

21. A. D. Crossland, "Estimates of Secondary Beam Yields from 20 GeV Electrons," Report No. SLAC-TN-66-45 (1966).

22. Cocconi, Koester, and Perkins, "Calculation of Particle Fluxes from Proton Synchrotrons of Energy 10 to 1000 GeV," LRL Report UCRL-10022 (1961) p. 167.

23. Boyarski et al. "Yields of Secondary Particles from 18-GeV Electrons," SLAC User's Handbook (1968).

24. Ranft, Nucl. Instr. Methods 48, 133 (1967).